Accepted Manuscript

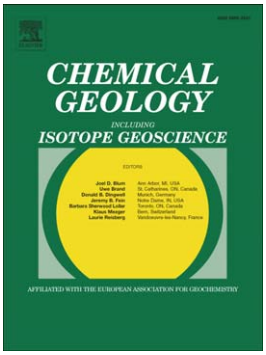

Experimental mineral dissolution in Berea Sandstone reacted with CO_2 or SO_2-CO_2 in NaCl brine under CO_2 sequestration conditions

G.K.W. Dawson, J.K. Pearce, D. Biddle, S.D. Golding

PII: S0009-2541(14)00444-6
DOI: doi: 10.1016/j.chemgeo.2014.10.005
Reference: CHEMGE 17369

To appear in: *Chemical Geology*

Accepted date: 2 October 2014

Please cite this article as: Dawson, G.K.W., Pearce, J.K., Biddle, D., Golding, S.D., Experimental mineral dissolution in Berea Sandstone reacted with CO_2 or SO_2-CO_2 in NaCl brine under CO_2 sequestration conditions, *Chemical Geology* (2014), doi: 10.1016/j.chemgeo.2014.10.005

This is a PDF file of an unedited manuscript that has been accepted for publication. As a service to our customers we are providing this early version of the manuscript. The manuscript will undergo copyediting, typesetting, and review of the resulting proof before it is published in its final form. Please note that during the production process errors may be discovered which could affect the content, and all legal disclaimers that apply to the journal pertain.

ACCEPTED MANUSCRIPT

Experimental mineral dissolution in Berea Sandstone reacted with CO_2 or SO_2-CO_2 in NaCl brine under CO_2 sequestration conditions

G.K.W. Dawson[a]*, J.K. Pearce[a,c], D. Biddle[b], S.D. Golding[a]

[a] School of Earth Sciences, The University of Queensland, QLD 4072, Australia
[b] School of Chemical Engineering, The University of Queensland, QLD 4072, Australia
[c] Collaborative Research Centre for Greenhouse Gas Technologies (CO2CRC), GPO Box 463, Canberra, ACT 2601, Australia

* Corresponding author. Tel.: +61 7 336 51180; fax: +61 7 336 51277.
E-mail addresses: g.dawson@uq.edu.au (G.K.W. Dawson), s.golding1@uq.edu.au (S.D. Golding).

Abstract

A comparison of the geochemical changes induced in sandstone by either pure or impure CO_2 at geological CO_2 storage conditions was investigated. Samples of Berea Sandstone were batch reacted in 1% w/v NaCl brine saturated with pure CO_2 or mixed SO_2-CO_2 gas for 360 hours at 50 ºC and 10 MPa. Geochemical analysis of incremental water samples showed increases in the concentrations of elements such as calcium, magnesium, iron, manganese, and silicon throughout experiments, likely being the products of carbonate and reactive silicate dissolution. Scanning electron microscope images taken of specific points of interest before and after batch reactions confirmed dissolution of carbonates, but showed no reaction for minerals such as K-feldspar. The magnitude of apparent mineral reaction was higher for the mixed gas SO_2-CO_2-brine experiment, with geochemical modelling also indicating greater dissolution of reactive silicates such as chlorite, and potential precipitation of amorphous silica.

Keywords

Geo-sequestration; CO_2; SO_2; Berea Sandstone; SEM-EDS

1. Introduction

Due to the high cost of gas purification, industrially sourced injection stream CO_2 may contain low levels of co-contaminants such as SO_2 (cf. Glezakou et al., 2012; Pearce et al., this issue), which when dissolved in groundwater will increase acidity beyond that of carbonic acid formed through CO_2 dissolution. Berea Sandstone was chosen to investigate mineral dissolution resulting from geochemical reactions with either CO_2 or mixed SO_2-CO_2 acidified brine. An approximately 0.05 mol% SO_2 in CO_2 gas mixture was used in this study to simulate a possible gas mixture from a coal combustion source (de Visser et al., 2008; IEAGHG, 2011; Saraji et al., 2014).

ACCEPTED MANUSCRIPT

Berea Sandstone has been used primarily in the context of the oil and gas sector to test various permeability scenarios, such as stress-dependent permeability (Baud et al., 2012), salinity dependent fines-inhibition of permeability (Azari and Leimkuhler, 1990; Hussain et al., 2013; Kia et al., 1987), CO_2 flow behaviour (Mohamed et al., 2012; Moore et al., 2004), multiphase fluid flow (Müller, 2011), reactive transport model simulations (Heidaryan et al., 2008; Ovaysi and Piri, 2013) and various geomechanical analyses (Dehler and Labuz, 2007; Feucht and Logan, 1990; Wissler and Simmons, 1985).

Very few studies have explored the impact of mixed SO_2-CO_2 gas injection upon geological materials, with the main focus on reactions with pure minerals (Garcia et al., 2012; Glezakou et al., 2012; Palandri et al., 2005; Wilke et al., 2012), and only a couple of studies investigated whole-rock chemical interactions (Kummerow and Spangenberg, 2011; Pearce et al., this issue). SO_2 when dissolved in groundwater may form either H_2SO_3 or H_2SO_4 (and H_2S) that are both stronger acids than H_2CO_3, and likely to result in enhanced mineral dissolution and porosity within the acidified zone around a mixed gas plume (Knauss et al., 2005; Xu et al., 2007). Over longer time periods and after pH buffering, dissolved sulfur species and CO_2 may be expected to be precipitated as sulfate and carbonate minerals, with consequently greater mineral trapping potential in the far-field.

2. Materials and methods

2.1. Experimental approach

In this study, sister sample 15 mm cubes of Berea Sandstone were reacted with either CO_2-brine or SO_2-CO_2-brine in a batch reactor, and the chemistry of the reaction water analysed to aid interpretation of potential mineralogical changes. Two different batch reactor systems were used, one of which allowed for incremental sampling of water chemistry. Modelling of incremental reaction water chemistry for selected samples was performed using the Geochemist's Workbench (GWB) to give some insight as to which mineral phases were major contributors to sample changes during experiments. Scanning Electron Microscope (SEM) surveys with Energy Dispersive Spectrometer (EDS) analyses were also done for selected points of interest on sample surfaces before and after batch reactor experiments.

The amount of SO_2 used for the mixed gas experiment was computed on the basis of having added 1 MPa of a mixture of 1 mol% SO_2 in CO_2 to the system and then added a further 4.5 MPa pCO_2 for a total gas volume of 0.131 L. The total moles of CO_2 was calculated using the Stryjek-Vera second modification of the Peng-Robinson equation of state (Stryjek and Vera, 1986a, b). This equated to 0.045 mol% SO_2 in CO_2.

ACCEPTED MANUSCRIPT

Samples were subject to gas-brine-rock interactions in custom-built geochemical batch reactors. Deoxygenated 1% w/v analytical grade NaCl solution (70 mL) was added to the reactors with the rock sample. The first cube (A) was reacted in a prototype 316 grade stainless steel batch reactor that did not allow for incremental sampling of vessel fluid during experiments (Dawson, 2012; Dawson et al., 2011; Massarotto et al., 2010). Subsequent samples (cubes B and C) were reacted in a new system based upon steel Parr reactors that did allow incremental fluid sampling (Figure 1), with custom built thermoplastic liners covering all metal parts to reduce corrosion as described in detail in Pearce et al. (this issue).

Vessels were purged of residual air with a low pressure N_2 flush. A HPLC pump was used to pressurize the prototype system prefilled with CO_2 to 6.0 ± 0.5 MPa and subsequently with brine to 10 MPa ± 0.5 MPa. For the new reactor, a Teledyne ISCO syringe pump (500HP) was used to pressurise the Parr vessels to 10.0 ± 0.5 MPa, initially with N_2 gas. Following an initial baseline water–rock soak for 2 days in the Parr vessels, 2 mL of solution phase was sampled, and N_2 gas subsequently replaced with either pure food grade CO_2 (Coregas) or ~ 0.05 mol% SO_2 in CO_2 pressurized with the syringe pump to 10 MPa ± 0.5 MPa.

Rock samples were reacted for 10 days immersed in the brine at 10 MPa and 50 ºC. Fluid samples were periodically taken for analysis. The short reaction time was chosen to represent conditions expected near an injection well-bore during initial flooding with CO_2 or mixed gas. In the immediate well-bore environment, gas-acidified groundwater is expected to be displaced by a gas-dominated phase thus terminating the main aqueous reactions in that region (e.g. André et al., 2011). Cubes A and B were reacted with supercritical CO_2 (sCO_2) dissolved in brine, and cube C with the SO_2 in sCO_2 mixture dissolved in brine. The gas:liquid ratio was ~ 2:1, and the water:rock ratio ~ 10:1.

Baseline levels of elements mobilised from the Parr reactors were determined by performing blank experiments at the same conditions as the experiments but without the rock sample.

2.2. Analytical methods

The solution chemistry of the geochemical batch reactors was periodically determined during the course of the experiments to monitor reaction progress. Solution pH was measured immediately with a TPS WP81 meter and probes with an error of ± 0.01 *ex situ* at the conclusion of experiments. Sampled aliquots of solution (~2 mL) were preserved with 2% v/v HNO_3 and (with the exception of the pure water blank) were diluted approximately 85X prior to analysis. An ICP-OES (Perkin Elmer Optima 3300 DV ICP-OES with a 3σ detection limit

ACCEPTED MANUSCRIPT

of 0.001 mg L^{-1}) was used to measure elemental concentrations of aqueous species in the experiment waters within an error range of ~ 5%.

SEM-EDS analyses were performed using a JEOL JSM-6460LA environmental SEM fitted with a Minicup EDS. The 6460 has low vacuum capability, which negated the need to coat sample surfaces with an electron conductive material in order to obtain high quality images of sample surfaces. For semi-quantitative EDS spot analyses, 1000x magnification was used, which equates to an area of electron beam-sample surface interaction of roughly 3 micrometres. Quantitative EDS analysis was not possible due to surface roughness. The brightness and contrast of SEM backscatter electron images give an indication of compositional differences within the samples, with brighter regions corresponding to heavier elements, and different minerals appearing as different shades of grey. However, surface charging and topography effects also contribute to image brightness and so visual appearance of the images can only be used as an approximate guide as to the different minerals present within the samples.

To assist identification of mineral dissolution and precipitation during the geochemical experiments, specific points of interest on sample surfaces were selected for precise pre and post reaction imaging with SEM (Figure 2). Low magnification images (30X) were sequentially taken across sample surfaces and numbered relative to one of the surface corners (e.g. #1 top left). Low accuracy EDS spot surveys were performed at low magnification and then any points of interest were imaged at successively higher magnifications (e.g. 200X, 500X, 1000X). Specific SEM stage rotation and x-y-z coordinates could be recorded for notable features within specific fields of view, additionally like-features were identified by eye in pre and post reaction views.

2.3. Berea Sandstone sample characterisation

Samples from the Berea Sandstone quarry, USA, were obtained from Australian National Low Emissions Coal R&D as part of a “round robin” comparison test of permeability measured in different laboratories. Surface fines resulting from the cutting of samples into cubes were removed by immersion in ethanol in open beakers within a well-ventilated sonic bath for 15 minutes, with samples then oven dried at 60 ºC for two days. Ethanol was used instead of water in order to avoid clay-water cation exchange reactions within the sample prior to experiments.

Sample specific mineralogy was obtained via whole rock and clay separate X-ray diffraction (XRD) analysis of a crushed sister sample; this is compared with literature data in Table 1 for the purpose of determining an initial mineralogy for modelling the geochemical experiments.

ACCEPTED MANUSCRIPT

Not all minerals present within samples are necessarily present in sufficient amount to be quantifiable by XRD. Moreover, trace minerals may be sufficiently reactive to contribute significantly to reaction water chemistry (Dawson, 2012). Rock sample surfaces were analysed using SEM-EDS to survey the sample mineralogy, especially trace minerals undetected or poorly detectable by XRD, and textural characteristics of the cubes.

SEM analysis indicated that the Berea Sandstone samples were predominantly quartzose, and contained feldspar grains and Fe-Ca-Mg-Mn-carbonate cements. Lesser amounts of dickite, kaolinite, micas and alteration products tentatively identified as chlorite, vermiculite, and smectite were also identified (Figure 3). The very small particle size and irregular shape and packing density of the clay-sized minerals made quantitative EDS determination of composition impossible. Pore space is partially occluded by clays and carbonate cements of variable composition, and sometimes also iron oxide/hydroxide. Very thin laminations of fine-grained material occur between the coarse quartz grain dominated layers. Whole-rock and clay separate XRD analysis of a sister-sample detected only trace amounts of reactive clay species (Table 1), likely because they were generally present in very thin depositional layers within the sample that amounted to only a very small fraction of total sample mass.

Standard petrographic analysis of a polished thin section found that the predominantly quartzose sandstone contains a few percent mica flakes (Figure 4). Haematite and clays, as well as carbonate cements to a lesser extent, occlude some of the porosity. Minor amounts of degraded feldspars and rare lithic fragments were also observed.

2.4. Geochemical modelling

The React and SpecE8 components of the Geochemist's Workbench (GWB) version 9 software package (Bethke and Yeakel, 2013) were used to model reaction pathways for experiments with samples B and C following addition of either CO_2 or mixed SO_2-CO_2.There were two main objectives for the modelling; a) identifying which mineral/s contributed to the observed increases in dissolved elements, especially silicon and aluminium, and b) to determine if the mineral fines observed to be partially occluding porosity play a significant role in any geochemical reactions. These were investigated by varying model input mineral mass, composition, and surface area in order to achieve the best modelled fits for the experimental data.

The initial modelled mineral composition is shown in Table 1. The measured concentration of elements in the experimental water during the nitrogen rock-brine soak step was used as the basis for the initial water composition used in the models (Table 2). Initial silicon concentration was below detection limit (owing to high analysis dilution factors) and therefore

ACCEPTED MANUSCRIPT

the background level of silicon measured during pure water reactor blanks was used in the solution basis after conversion to concentration of SiO_2. The system was balanced with respect to chlorine and bicarbonate in SpecE8.

The CO_2 fugacity was calculated on the basis of the pressure (10 MPa), temperature (50 ºC), and salinity (1% w/v NaCl solution) (Duan and Sun, 2003; Duan et al., 2006). A modified version of the EQ3/6 thermodynamic database for aqueous and mineral species (Bethke and Yeakel, 2013; Delany and Lundeen, 1989) was utilised. Script files (Pearce et al., this issue) containing the kinetic input data in Table 3 were used for all minerals except rhodochrosite, for which the inbuilt GWB rate law was employed using an initial rate constant of $4*10^{-13}$ mol/cm^{2}sec. Due to the limitations of the modelling software used, rather then defining SO_2 behaviour together with CO_2 in the model basis, 0.06 mol/kg SO_2 was added to the cube C SO_2-CO_2 model as a reactant with a cut-off of 0.033 mol/kg to match the experimentally determined dissolved sulfate concentrations (calculated by converting measured dissolved S assuming this was sulfate) over time.

The exact composition of some minerals was varied (Table 4) in order for the models to better match experimentally determined dissolved element concentration profiles over time. A range of compositions of minerals such as the carbonate cement and fine grained phyllosilicates was indicated by SEM-EDS analyses. Accordingly, the composition of chlorite used in each model was different due to better matches for the respective Fe and Mg concentration profiles depending upon which type of chlorite was used. Similarly, different composition ankerite, and differing proportions and surface areas of all relevant carbonate minerals were used in each model in order to obtain the best fits with experimental data.

The quartz mass was varied in order to balance the sum of mineral masses relative to an initial sample mass of 6.8 g. Mineral masses used in the models were based upon measured and literature XRD data as well as standard petrography and SEM-EDS analyses of sample surfaces (Table 1). Both surface area and to some extent mineral mass were manipulated as variables to constrain the modelled concentration profiles for elements. As experiments were performed on a cube of Berea Sandstone rather than crushed rock samples not all minerals present may have been accessible to reactive fluids, e.g. where cements or clays covered grains, and the exact proportions of minerals present could have varied between samples. Initial surface areas were increased as indicated in Table 3.

3. Results

3.1. Experimental water chemistry

ACCEPTED MANUSCRIPT

The solution pH at the termination of the Berea SO_2-CO_2-brine experiment was 2.69, significantly lower than in the pure CO_2-brine reactions (pH 5.77 or 4.42), as shown in Table 2. Analysis of incremental water samples collected periodically during the experiments showed increases in the concentration of dissolved elements in solution with time (Table 2). The major aqueous elements for both CO_2-brine and SO_2-CO_2-brine experiments included Ca, Fe, and Mg (Figure 5a).

Over three times the concentration of Fe was measured in solution during Berea SO_2-CO_2-brine reaction (345 mg/kg) compared to Berea CO_2-brine reaction (114 mg/kg) (Table 2 and Figure 5 a). The concentration of dissolved Al was also highly elevated (~ 30 times) and Si ~ 2 times higher in the SO_2-CO_2-brine experiment compared to the pure CO_2 experiment after 12 days reaction (Figure 5 b). On the other hand, Ca, Mg and Mn concentrations were only slightly elevated during the SO_2-CO_2 experiment (Figure 5a,b).

The measured concentrations of aqueous Ca, Fe, Mg, Si, Mn, Cu, Pb, and V were higher for all rock sample experiments relative to blank levels, and hence probably originated from rock dissolution. The values for Cu, Pb, V fluctuate due to these being at the lower limits of the analysis. The concentrations of As, B, Be, Co, Se, and Ti were below the respective detection limits for these elements. Significant sample dilution to bring major element concentrations within calibration measurements may have contributed to trace element concentrations dropping below detection. Ba, Cd, K, Li, Na, P, and Sr concentrations did not exceed background levels during the rock sample experiments and were above the respective detection limits.

For the CO_2-brine experiments with cubes A and B, the concentrations of Al, Mo, Ni, S, and Zn were similar to the background levels of the reactor systems and so it is possible that they resulted from a combination of fluid-rock interaction, background residue from previous experiments, and/or reactor corrosion (Table 2). Some of the Cr, Fe, Ni, V, and Zn mobilised during the SO_2-CO_2 experiment with cube C probably did originate from reactor material, but the amount of aqueous iron present by the end of the experiment was at least an order of magnitude greater than the SO_2-CO_2-brine blank with no sample.

The observed dissolved sulfur increase over time to 730 mg/kg in the SO_2-CO_2 experiment was likely due mostly to equilibration between gaseous and aqueous SO_2 subsequently converted into aqueous sulfate (partly through oxidation by Fe oxides present in the rock).

ACCEPTED MANUSCRIPT

3.2. Experimental rock surface changes

Comparison of SEM images taken before and after experiments (Figure 6 a-d) indicated dissolution of carbonate cement occurred during all experiments. There was complete removal of surficial carbonate cement during the SO_2-CO_2-brine experiment (e.g. Figure 6d), whereas some carbonate cement remained visible near the surface of cubes A and B after pure CO_2 reactions (e.g. Figure 6b). This observation correlates well with the fact that the concentrations of aqueous elements measured for the SO_2-CO_2 experiment were greater than for the CO_2 experiments. The observed increases in aqueous Mn throughout all sample experiments (Figure 5b) likely correlated with dissolution of the carbonate cements. SEM-EDS analyses pre-reaction showed all carbonate cements to contain Mn in addition to varying amounts of Ca, Fe, and Mg (e.g. Figure 4f).

SEM and XRD indicated that the Berea Sandstone samples contained trace chlorite, vermiculite and smectite (Figure 4, Table 1). Evidence of corrosion of silicates was not observed in post reaction SEM. This, however, may be owing to an inability to locate trace reactive silicates on the surfaces of reacted cubes pre/post reaction. Loss of fine material from between the framework grains of the samples was observed; however, it was not clear whether this was due to chemical reaction or physical mobilisation of fines from the cube surface. The surfaces of large aluminosilicate grains (e.g. K-feldspar Figure 6f) showed no changes following the batch reactor experiments.

3.3. GWB mineral reaction modelling

The incremental water chemistry of the batch reactor experiments for cubes B (Berea CO_2-brine reaction) and C (Berea SO_2-CO_2-brine reaction) were modelled using the Geochemist's Workbench (GWB) with respect to mineral and water chemistry. Model outputs of dissolved element concentration (with experimental results plotted for comparison as icons), minerals dissolved and precipitated, and solution pH are shown in Figures 7 and 8. The modelled element concentrations in solution show a good match with the experimental data for most elements. Carbonate mineral dissolution was observed in both models with CO_2 or SO_2-CO_2-brine reaction. A greater mass of ankerite reacted in the SO_2-CO_2-brine model than in the pure CO_2-brine model (Table 6 and 7). The mass of chlorite decreased more significantly than other silicates in both models, indicating this was the most reactive silicate. In the SO_2-CO_2 model a greater mass of chlorite, kaolinite and K-feldspar dissolved than in the CO_2 brine model.

Elemental S precipitated in the SO_2-CO_2-brine model, resulting in a flattening of the sulfate concentration with time. Quartz precipitation is unlikely to have happened in experiments at

ACCEPTED MANUSCRIPT

the overall low pH observed, but together with chalcedony was a proxy to reduce silica concentration in solution as the leaching of Fe and Al from reactive silicates to leave a silica-rich layer cannot be modelled. Precipitation of an aluminium-rich phase during the cube B experiment was plausible given that measured Al concentration remained fairly constant over time. The model favoured diaspore precipitation over boehmite and gibbsite, which is in agreement with experiments performed over a similar pH range by Peryea and Kittrick (1988) that found diaspore was the most stable phase.

Solution pH in the Berea CO_2-brine model was initially ~ 3 and then increased to ~ pH 4.5 after 10 days in reasonable agreement with experimental pH. In the Berea SO_2-CO_2-brine model, pH reduced from ~ 3 to ~ pH 2.4 after 10 days in reasonable agreement with the pH measured at the conclusion of the experiment. This was in spite of the fact that pH measurements were *ex situ*, although given that the waters were still degassing via bubbling they were still gas-saturated during pH measurements.

As the current experiments use batch rather than flow reactors, the exchange of aqueous fluid in the rock pores with dissolved CO_2 (and SO_2) saturated brine may be diffusion limited. Therefore it is possible the reactive fluid did not interact with minerals below the surface of the Berea cubes if pore networks were not connected. The model outputs and high reactive surface areas needed indicate that a large portion of the minerals were likely in contact with low pH fluid and reacted. Experimental work using similar conditions with micro CT imaging in this issue has indicated reactive fluids penetrate to the centre of 3mm diameter sandstone sub-plugs (Farquhar et al., this issue). Given the large grain size and higher porosity of the Berea sandstone, it is expected that some fluid penetration did occur; however, further work outside the scope of this study would be necessary to determine the full extent of fluid penetration and sample reaction.

4. Discussion

The magnitude of the concentration of the dissolved elements Al, Ca, Cr, Fe, Mg, Mn, Mo, Ni, Pb, Si, V, and Zn was higher in the SO_2-CO_2 experiment with cube C compared with the CO_2-only experiments with cubes A and B (Table 5). Dissolved SO_2 being converted to sulfurous and/or sulfuric acid, that are much stronger acids than carbonic acid, would have contributed to enhanced acid activated dissolution of minerals in cube C (Knauss et al., 2005; Xu et al., 2007). The pH in the SO_2-CO_2-brine experiment was lower than in pure CO_2 reactions indicating formation of sulfuric acid did occur. This is in agreement with previous experiments reacting pure mineral separates with pure or impure CO_2 and brine (Wilke et al., 2012), where the addition of SO_2 resulted in a solution pH ~ 1-3 and reaction of silicates (e.g. biotite and albite).

ACCEPTED MANUSCRIPT

In the current experiments, the concentrations of Al, Fe and Si in solution were much higher in the case of the SO_2-CO_2-brine reaction with Berea Sandstone in comparison with CO_2-brine reactions. This suggests that silicate dissolution/leaching was enhanced due to the lower pH. Incremental fluid samples taken periodically throughout the experiments generally show an initial rapid increase in concentration of most elements following initial exposure to reaction fluids, suggesting that primarily dissolution of mineral fines is occurring during this time. The large modelled surface areas required for minerals such as chlorite and carbonates in order to match the experimentally determined concentrations of aqueous species confirms the key role played by mineral fines in the water-rock interactions that took place.

The SEM surveys pre and post reaction (Figure 6) coupled with the water chemistry data indicate that carbonate cement dissolution contributed to the measured increases in aqueous elements over time for all rock sample reactions. Static geochemical modelling for Berea cubes B and C with CO_2 or SO_2-CO_2-brine confirmed carbonate dissolution, which appeared more extensive with the presence of SO_2. Wilke et al. (2012) also observed high reactivity of carbonates in the presence of SO_2 in good agreement with the current work. They observed ~ 10 times greater Ca concentration in solution with SO_2 present in comparison to pure CO_2 reaction. Significant corrosion of dolomite and calcite was observed in SEM post SO_2-CO_2-brine reaction by Wilke et al. (2012).

Chlorite was identified as likely being the most reactive aluminosilicate phase (Figures 7 and 8). Previous work has indicated that chlorite undergoes incongruent dissolution at acidic pH, with preferential leaching of Fe and Al leaving a silica-rich layer (Baker et al., 1993; Brandt et al., 2003). Higher silicate corrosion (albite) was also observed in the presence of SO_2 in the work of Wilke et al. (2012). This effect is not directly accounted for in the GWB model for dissolution of chlorite, and is likely why chalcedony and quartz precipitation in the models was necessary as a proxy to reduce the silica concentration in solution and attempt to match experimentally observed values.

It is possible that the experimental pH was more acidic than modelled for the majority of the experiment. This could also explain why the SO_2-CO_2-brine model for cube C precipitated chalcedony and therefore modelled aqueous silicon failed to match the measured increases with time. The only reliable pH measurements for the experiments were made *ex situ* at the conclusion of the experiment where CO_2 degassing means they represent a maximum value, although the measured values did match well with the modelled pH values.

Mineral surface areas of the carbonates as well as chlorite had to be increased substantially above initial values chosen in order to model the initial reaction water chemistry, which

ACCEPTED MANUSCRIPT

suggests that a lot of the reacted material was most likely mineral fines. Experimentally, there would likely have been a continuum of different surface areas for each mineral, with mass apportioned among them rather than the single surface area, mass, and composition values used in the models. Moreover, not all mineral matter present within the cubes would have interacted significantly with the reaction water. This is partly due to not all minerals being linked via interconnected porosity to the cube surfaces, but also because of diffusion effects resulting from the static nature of the experiments.

An alternative modelling approach would have been to split the models into two phases, an initial model in which mainly fines were reacting and then a second model continuing on from it for which lower surface area minerals began to react (Farquhar et al., this issue). Alternatively, the two approaches could have been combined into a single model in which minerals were included more than once, but with different masses and surface areas for each entry. However, given that the purpose of the modelling done for this study was to confirm which phases were most likely involved in geochemical reactions, and whether mineral fines played a key role in reactions, the current modelling is sufficient.

Reactive transport models of other studies have indicated that enhanced dissolution during SO_2-CO_2-brine-rock interactions compared with CO_2-brine-rock would ultimately result in enhanced precipitation of carbonates, sulfates and potentially even sulfides once the pH became sufficiently alkaline (Knauss et al., 2005; Xu et al., 2007). Therefore there is likely greater potential for mineral trapping of CO_2 for the mixed SO_2-CO_2-brine scenario compared with pure CO_2-brine. However, the low quantity of carbonate present within the Berea samples A, B, and C and the short timeframe of experiments precluded any significant precipitation of minerals being observed.

5. Conclusions

Incremental fluid concentrations show an initial increase in most measured major and trace elements over time, with greater concentrations of aqueous elements measured for SO_2-CO_2-brine experiments in comparison to CO_2-brine experiments. Comparison between SEM images of selected areas of interest pre and post reactions showed that dissolution of carbonate cements occurred whereas low surface area grains of K-feldspar showed no reaction. GWB modelling indicated that reaction of chlorite likely occurred during all experiments, though this was not directly observed via SEM due to the difficulty in locating pure chlorite flakes of sufficient size for semi-quantitative SEM-EDS analysis. Geochemical modelling also indicated that the majority of minerals that took part in reactions during the short term experiments of this study were likely high surface area fines.

ACCEPTED MANUSCRIPT

Acknowledgments

The authors wish to acknowledge financial assistance provided by Australian National Low Emissions Coal Research and Development (ANLEC R&D). ANLEC R&D is supported by Australian Coal Association Low Emissions Technology Limited and the Australian Government through the Clean Energy Initiative. Julie Pearce acknowledges the funding provided by the Commonwealth of Australia and industry sponsors through the CO2CRC Program. Thanks to Marietjie Mostert and Alison Law for assistance with laboratory analyses, and to the two anonymous reviewers for helpful comments and suggestions. We acknowledge the facilities, and the scientific and technical assistance, of the Australian Microscopy and Microanalysis Research Facility at the Centre for Microscopy and Microanalysis, The University of Queensland.

References

André, L., Azaroual, M., Peysson, Y., Bazin, B., 2011. Impact of porous medium desiccation during anhydrous CO_2 injection in deep saline aquifers: Up scaling from experimental results at laboratory scale to near-well region. Energy Procedia 4, 4442-4449.

Azari, M., Leimkuhler, J., 1990. Completion Fluid Invasion Simulation and Permeability Restoration by Sodium-and Potassium-Based Brines, SPE Formation Damage Control Symposium.

Baker, J.C., Uwins, P.J.R., Mackinnon, I.D.R., 1993. ESEM study of authigenic chlorite acid sensitivity in sandstone reservoirs. Journal of Petroleum Science and Engineering 8, 269-277.

Baud, P., Meredith, P., Townend, E., 2012. Permeability evolution during triaxial compaction of an anisotropic porous sandstone. Journal of Geophysical Research: Solid Earth 117, B05203.

Bethke, C.M., Yeakel, S., 2013. The Geochemist's Workbench Realease 9.0: Reaction Modeling Guide. Aqueous Solutions, LLC, Champaign, Illinois.

Brandt, F., Bosbach, D., Krawczyk-Bärsch, E., Arnold, T., Bernhard, G., 2003. Chlorite dissolution in the acid ph-range: a combined microscopic and macroscopic approach. Geochimica et Cosmochimica Acta 67, 1451-1461.

Dawson, G.K.W., 2012. Carbon dioxide sequestration in coal: The relationships between coal structure, texture, and mineralogy, and the role of mineral reactivity with carbonic acid, School of Earth Sciences. The University of Queensland, Brisbane, p. 235.

Dawson, G.K.W., Golding, S.D., Massarotto, P., Esterle, J.S., 2011. Experimental supercritical CO_2 and water interactions with coal under simulated *in situ* conditions. Energy Procedia 4, 3139-3146.

ACCEPTED MANUSCRIPT

de Visser, E., Hendriks, C., Barrio, M., Mølnvik, M.J., de Koeijer, G., Liljemark, S., Le Gallo, Y., 2008. Dynamis CO_2 quality recommendations. International Journal of Greenhouse Gas Control 2, 478-484.

Dehler, W., Labuz, J., 2007. Stress Path Testing of an Anisotropic Sandstone. Journal of Geotechnical and Geoenvironmental Engineering 133, 116-119.

Delany, J.M., Lundeen, S.R., 1989. The LLNL thermochemical database. Lawrence Livermore National Laboratory Report UCRL-21658.

Deshpande, S.R., 2006. Geochemical Simulation of Laboratory CO_2 Sequestration Experiments. University of Oklahoma.

Duan, Z., Sun, R., 2003. An improved model calculating CO_2 solubility in pure water and aqueous NaCl solutions from 273 to 533 K and from 0 to 2000 bar. Chemical Geology 193, 257-271.

Duan, Z., Sun, R., Li, D.D., Hu, J.W., Zhu, C., Chou, I.M., 2006. Thermodynamic Properties of the H_2O-CO_2-NaCl System, Zhenhao Duan Research Group, Institute of Geology and Geophysics, Chinses Academy of Sciences.

Farquhar, S.M., Pearce, J.K., Dawson, G.K.W., Golab, A., Sommacal, S., Kirste, D., Biddle, D., Golding, S.D., this issue. A fresh approach to investigating CO_2 storage: Experimental CO_2-water-rock interactions in a low-salinity reservoir system. Submitted to Chemical Geology.

Feucht, L.J., Logan, J.M., 1990. Effects of chemically active solutions on shearing behavior of a sandstone. Tectonophysics 175, 159-176.

Garcia, S., Rosenbauer, R.J., Palandri, J., Maroto-Valer, M.M., 2012. Sequestration of non-pure carbon dioxide streams in iron oxyhydroxide-containing saline repositories. International Journal of Greenhouse Gas Control 7, 89-97.

Glezakou, V.-A., Peter McGrail, B., Todd Schaef, H., 2012. Molecular interactions of SO_2 with carbonate minerals under co-sequestration conditions: A combined experimental and theoretical study. Geochimica et Cosmochimica Acta 92, 265-274.

Heidaryan, E., Enayati, M., Mokhtari, B., 2008. Laboratory Investigations into the Reactive Transport Module of Carbon Dioxide Sequestration and Geochemical Simulation. Petroleum Society of Canada.

Hussain, F., Zeinijahromi, A., Bedrikovetsky, P., Badalyan, A., Carageorgos, T., Cinar, Y., 2013. An experimental study of improved oil recovery through fines-assisted waterflooding. Journal of Petroleum Science and Engineering 109, 187-197.

IEAGHG, 2011. Effects of Impurities on Geological Storage of CO_2, 2011/04 ed.

Kia, S.F., Fogler, H.S., Reed, M.G., Vaidya, R.N., 1987. Effect of Salt Composition on Clay Release in Berea Sandstones.

ACCEPTED MANUSCRIPT

Knauss, K.G., Johnson, J.W., Steefel, C.I., 2005. Evaluation of the impact of CO_2, co-contaminant gas, aqueous fluid and reservoir rock interactions on the geologic sequestration of CO_2. Chemical Geology 217, 339-350.

Kummerow, J., Spangenberg, E., 2011. Experimental evaluation of the impact of the interactions of CO_2-SO_2, brine, and reservoir rock on petrophysical properties: A case study from the Ketzin test site, Germany. Geochemistry, Geophysics, Geosystems 12, Q05010.

Massarotto, P., Golding, S.D., Bae, J.S., Iyer, R., Rudolph, V., 2010. Changes in reservoir properties from injection of supercritical CO_2 into coal seams -- A laboratory study. International Journal of Coal Geology 82, 269-279.

Mohamed, I.M., He, J., Nasr-El-Din, H.A., 2012. Carbon Dioxide Sequestration in Sandstone Aquifers: How Does It Affect the Permeability?, Carbon Management Technology Conference, Texas A&M University.

Moore, J.R., Glaser, S.D., Morrison, H.F., Hoversten, G.M., 2004. The streaming potential of liquid carbon dioxide in Berea sandstone. Geophysical Research Letters 31, L17610.

Müller, N., 2011. Supercritical CO_2-Brine Relative Permeability Experiments in Reservoir Rocks—Literature Review and Recommendations. Transport in Porous Media 87, 367-383.

Ovaysi, S., Piri, M., 2013. Pore-scale dissolution of CO_2 and SO_2 in deep saline aquifers. International Journal of Greenhouse Gas Control 15, 119-133.

Palandri, J.L., Rosenbauer, R.J., Kharaka, Y.K., 2005. Ferric iron in sediments as a novel CO_2 mineral trap: CO_2-SO_2 reaction with hematite. Appl. Geochem. 20, 2038-2048.

Pearce, J.K., Dawson, G.K.W., Golding, S.D., this issue. SOx and supercritical CO_2 short-term effects upon geological samples under simulated *in situ* condtions. Submitted to Chemical Geology.

Peryea, F.J., Kittrick, J.A., 1988. Relative solubility of corundum, gibbsite, boehmite, and diaspore at standard state conditions. Clays and Clay Minerals 36, 391-396.

Saraji, S., Piri, M., Goual, L., 2014. The effects of SO_2 contamination, brine salinity, pressure, and temperature on dynamic contact angles and interfacial tension of supercritical CO_2/brine/quartz systems. International Journal of Greenhouse Gas Control 28, 147-155.

Stryjek, R., Vera, J.H., 1986a. PRSV2: A cubic equation of state for accurate vapor-liquid equilibria calculations. The Canadian Journal of Chemical Engineering 64, 820-826.

Stryjek, R., Vera, J.H., 1986b. PRSV: An improved Peng-Robinson equation of state for pure compounds and mixtures. The Canadian Journal of Chemical Engineering 64, 323-333.

Van Den Abeele, K.E.A., Carmeliet, J., Johnson, P.A., Zinszner, B., 2002. Influence of water saturation on the nonlinear elastic mesoscopic response in Earth materials and the

ACCEPTED MANUSCRIPT

implications to the mechanism of nonlinearity. Journal of Geophysical Research: Solid Earth 107, ECV 4-1-ECV 4-11.

Wilke, F.D.H., Vásquez, M., Wiersberg, T., Naumann, R., Erzinger, J., 2012. On the interaction of pure and impure supercritical CO_2 with rock forming minerals in saline aquifers: An experimental geochemical approach. Applied Geochemistry 27, 1615-1622.

Wissler, T.M., Simmons, G., 1985. The physical properties of a set of sandstones—Part II. Permanent and elastic strains during hydrostatic compression to 200 MPa. International Journal of Rock Mechanics and Mining Sciences & Geomechanics Abstracts 22, 393-406.

Xu, T., Apps, J.A., Pruess, K., Yamamoto, H., 2007. Numerical modeling of injection and mineral trapping of CO_2 with H_2S and SO_2 in a sandstone formation. Chemical Geology 242, 319-346.

Figures

Figure 1: Illustration of Parr reactor showing thermoplastic liner.

Figure 2: Illustration of method of locating and taking images of the same regions of interest on sample surfaces pre and post reaction. a) Low magnification ranging view for locating area of interest (in box); b) higher magnification image of area of interest; c) EDS spectra of unreactive zircon grain used to assist locating positions of areas of interest; d) EDS spectra of siderite cement between quartz grains within area of interest on Berea Sandstone. Z = zircon, Q = quartz, S = siderite.

Figure 3: SEM back-scatter electron images of unreacted Berea Sandstone, a) K-feldspar, kaolin, quartz; b) K-feldspar, perthitic K-feldspar, quartz ; c) Vermiculite and chlorite, degraded K-feldspar, quartz; d) carbonate cement, quartz; e) dickite between quartz grains; f) EDS spectra of Fe-dolomite on quartz in d). D = dickite, Fe-D = ferroan dolomite, kA = kaolinite, kF = K-feldspar, pkF = perthitic K-feldspar, dM = degraded Mg-K-Fe-mica.

Figure 4: Muscovite flake between quartz grains, cross polarized light 20X magnification.

Figure 5: Selected measured major (a) and minor (b) aqueous ion concentrations (mg/kg) during the SO_2-CO_2 experiment with cube C indicated by open symbols and dashed lines, and the pure CO_2 experiments with cube B indicated by solid symbols and lines. Point zero on the charts refers to the concentration of a given element present within the brine used for the experiment. The approximate error in the concentration values is 5%.

ACCEPTED MANUSCRIPT

Figure 6: Pre and post reaction SEM images of minerals on the Berea surface. a) Pre CO_2 reaction siderite and haematite (white) between quartz grains (grey), b) post CO_2 reaction in same area as a) with siderite corroded, c) pre SO_2-CO_2-brine reaction siderite, and quartz. d) post SO_2-CO_2-brine reaction, same area as c) with extensive siderite corrosion exposing hematite. (e) K-feldspar surface, and (f) same area as e) and post SO_2-CO_2-brine exposure. H = haematite, kF = K-feldspar, Q = quartz, S = siderite.

Figure 7: The geochemical modelling outputs (lines) are indicated for CO_2-brine Berea Sandstone cube B, with experimentally measured concentrations indicated as icons. With a) and b) dissolved element concentration evolution with time, c) d) e) changes in mineral mass over time, f) change in solution pH. Day zero is when CO_2 was added to system.

Figure 8: The model outputs of Berea SO_2-CO_2-brine reaction (lines) are indicated, with experimentally measured concentrations indicated as icons. With a), b) and c) element concentration evolution with time, d) e) changes in minerals over time, f) change in solution pH. Day zero is when SO_2-CO_2 was added to system.

Legends

(For table 1)

[a] Literature XRD mineral data averaged from Azari and Leimkuhler (1990), Deshpande (2006), Van Den Abeele et al. (2002) and Wissler and Simmons (1985). n.d. = not detected. Approximate error for each XRD value is +/- 5%.

(For table 4)

[a]Rhodochrosite was included to account for the manganese in carbonate cements observed by SEM-EDS.

(For table 5)

[a] <DT means below detection limit. The concentrations of As, B, Be, Co, Ti, and Se were below detection limit for all analyses.

(For tables 6 and 7)

[a] Negative values indicate precipitation.

ACCEPTED MANUSCRIPT

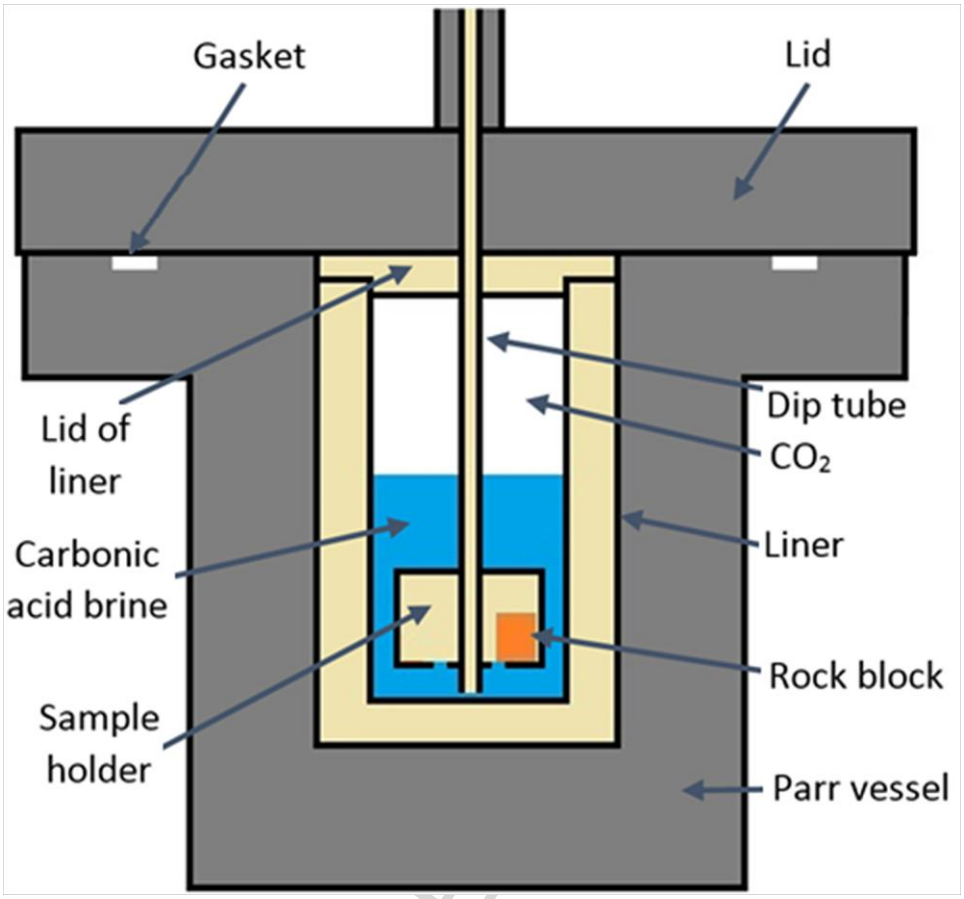

Figure 1

ACCEPTED

ACCEPTED MANUSCRIPT

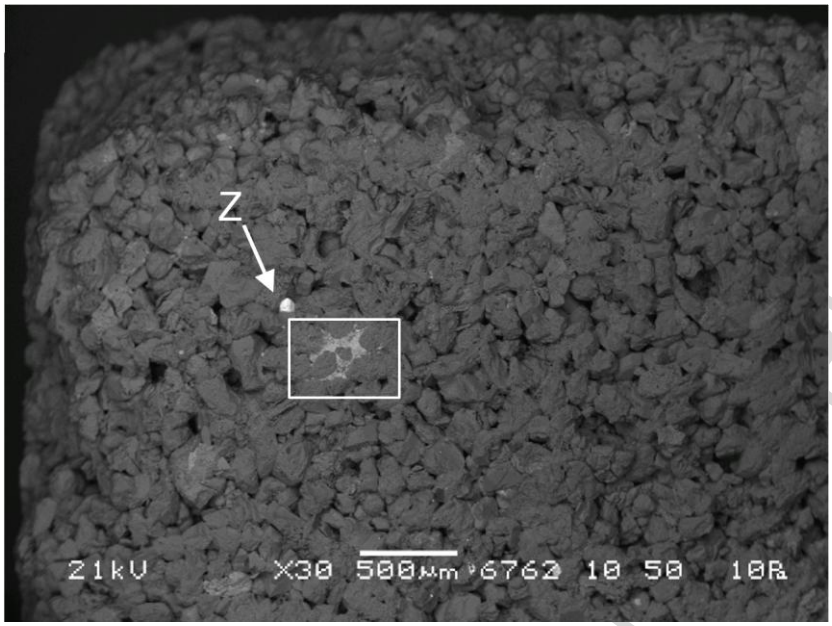

Figure 2a

ACCEPTED MANUSCRIPT

ACCEPTED MANUSCRIPT

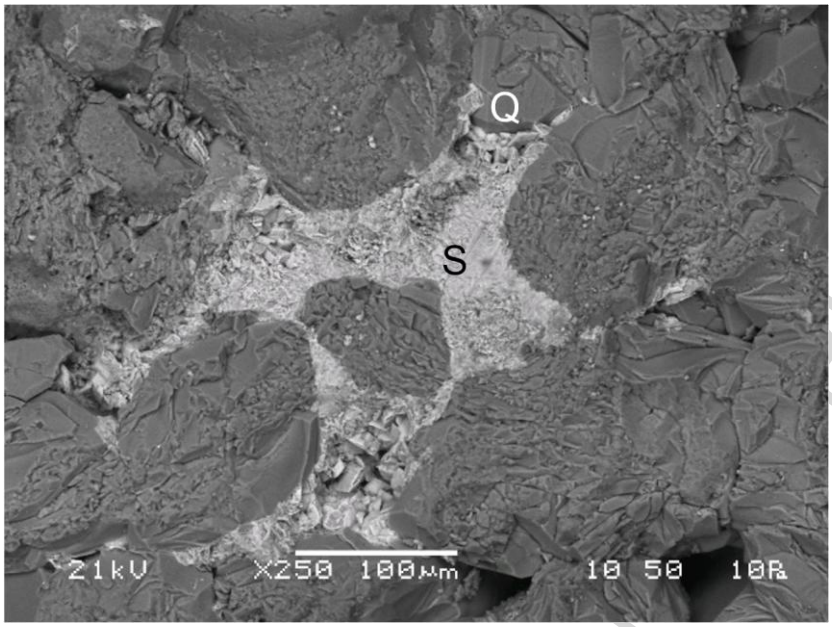

Figure 2b

ACCEPTED MANUSCRIPT

ACCEPTED MANUSCRIPT

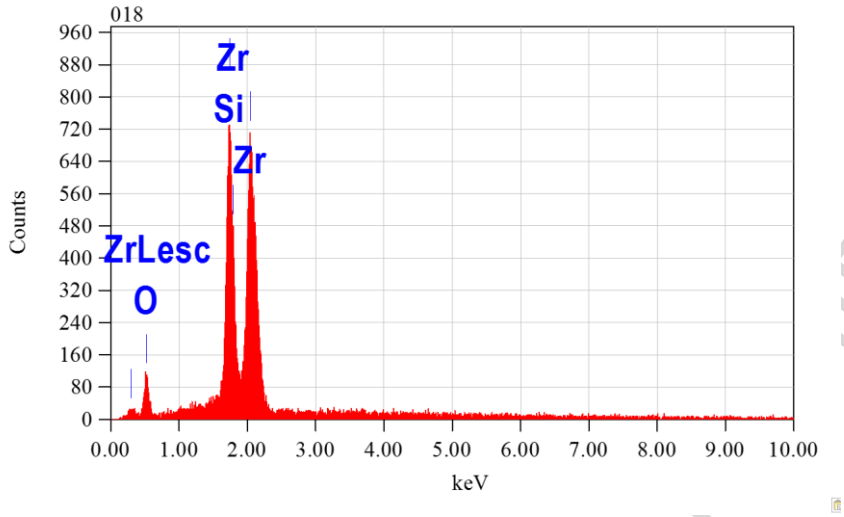

Figure 2c

ACCEPTED MANUSCRIPT

ACCEPTED MANUSCRIPT

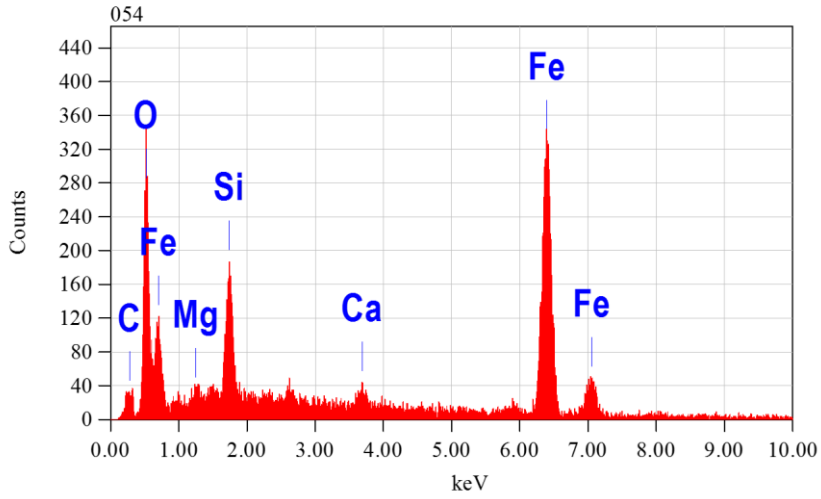

Figure 2d

ACCEPTED MANUSCRIPT

ACCEPTED MANUSCRIPT

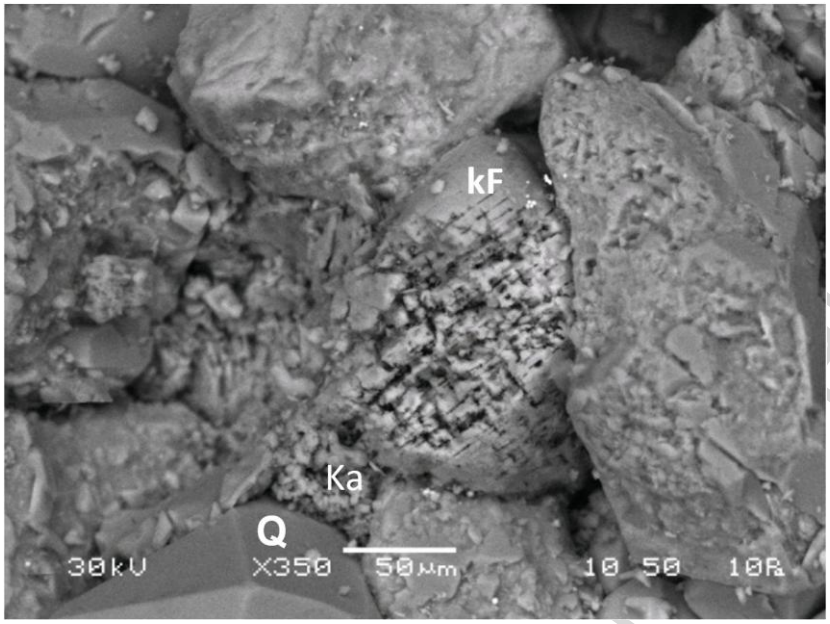

Figure 3a

ACCEPTED MANUSCRIPT

ACCEPTED MANUSCRIPT

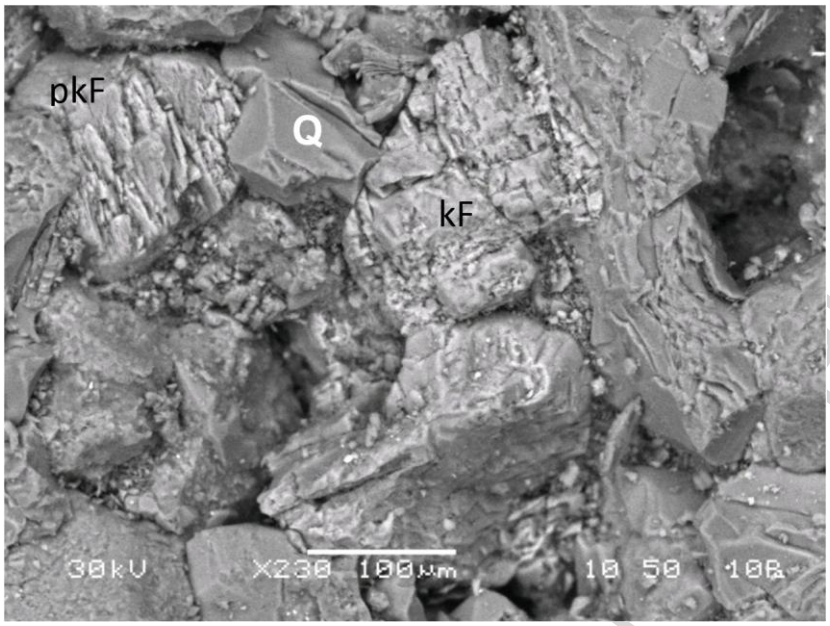

Figure 3b

ACCEPTED MANUSCRIPT

ACCEPTED MANUSCRIPT

Figure 3c

ACCEPTED MANUSCRIPT

ACCEPTED MANUSCRIPT

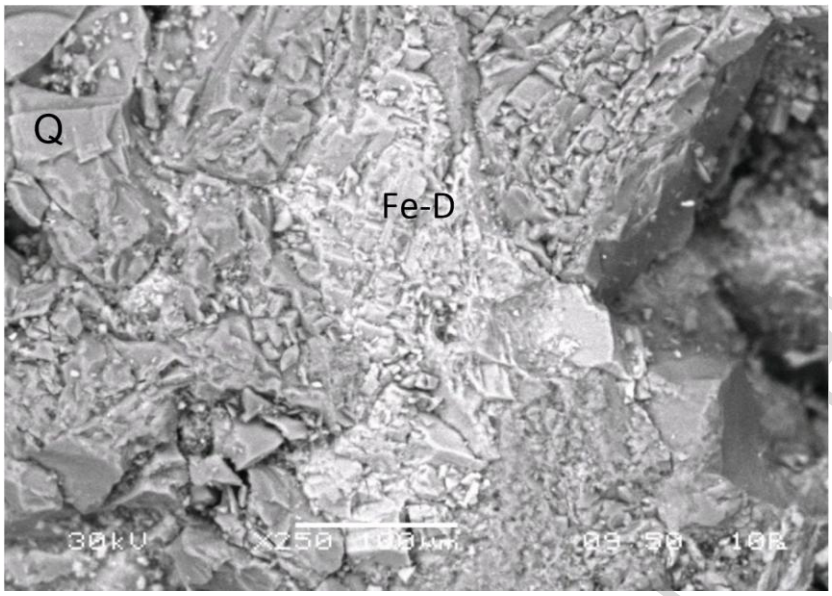

Figure 3d

ACCEPTED MANUSCRIPT

ACCEPTED MANUSCRIPT

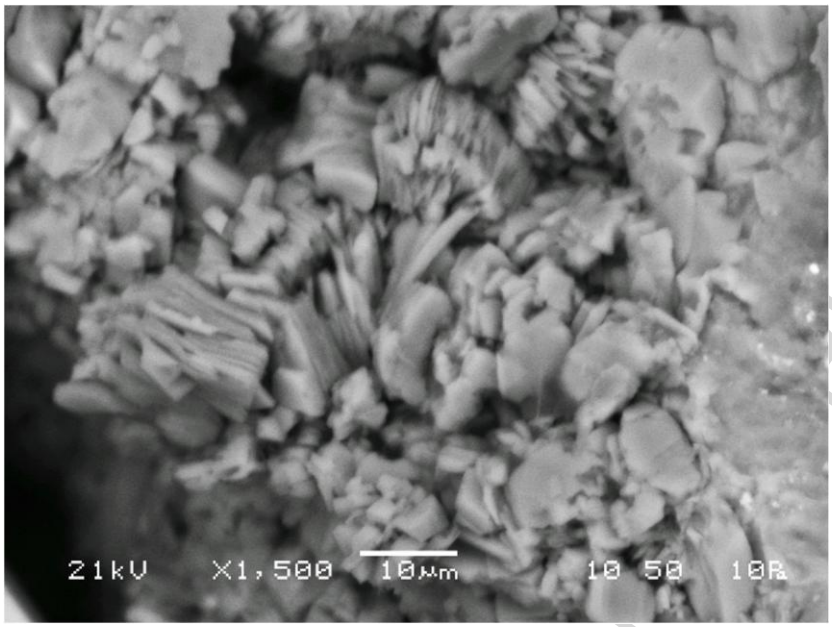

Figure 3e

ACCEPTED MANUSCRIPT

ACCEPTED MANUSCRIPT

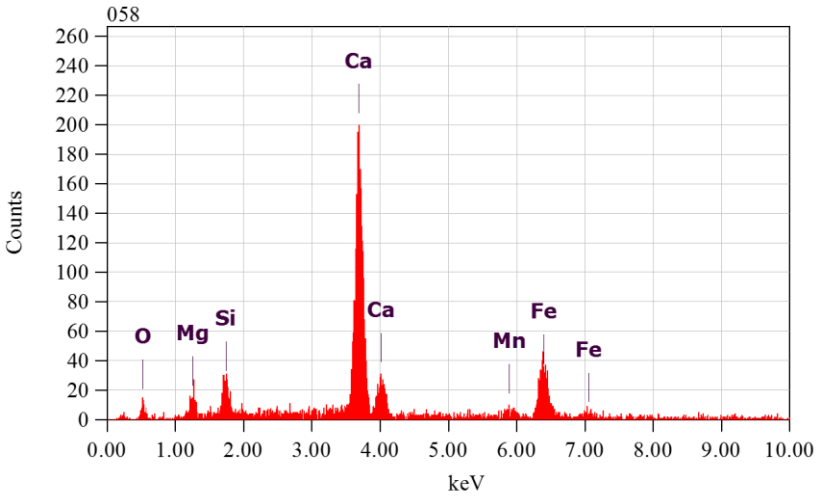

Figure 3f

ACCEPTED MANUSCRIPT

ACCEPTED MANUSCRIPT

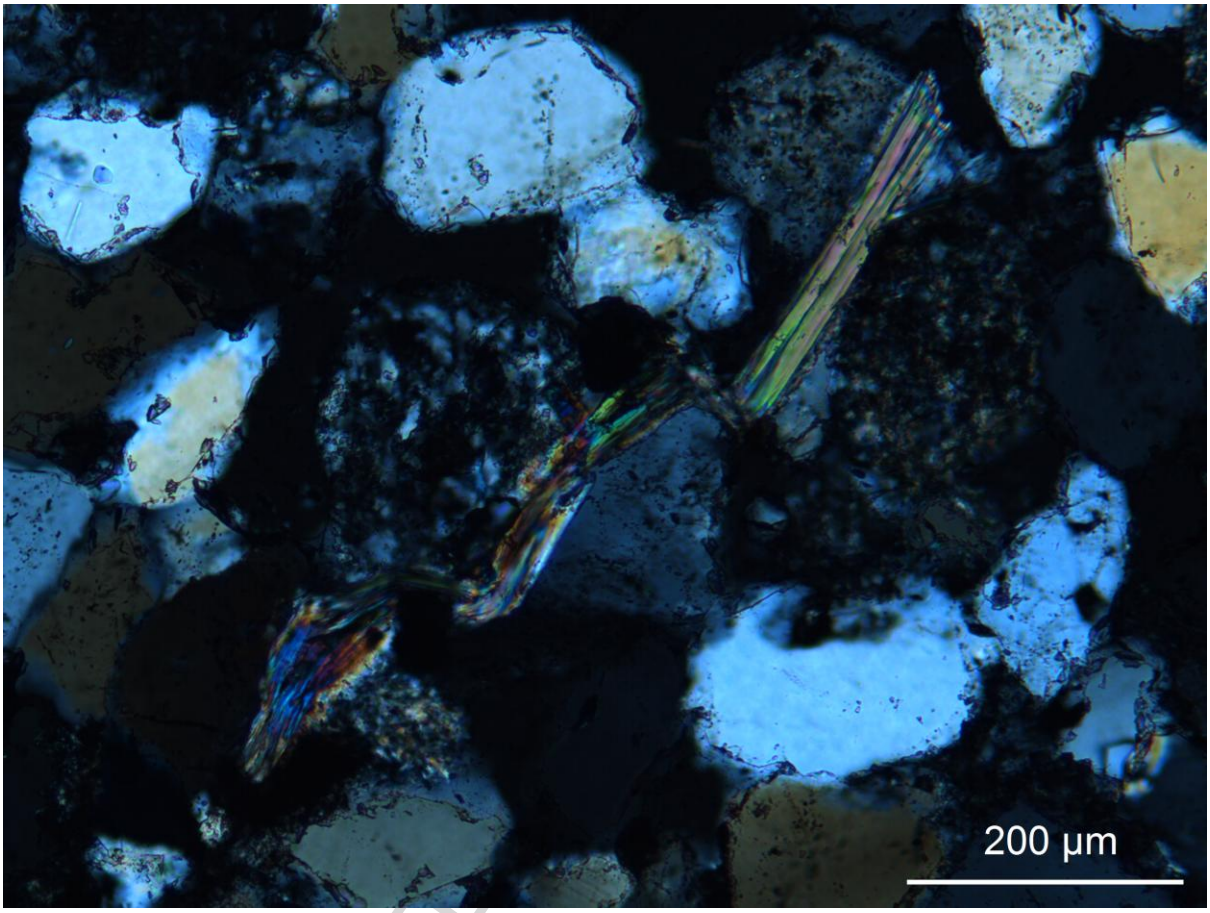

Figure 4

ACCEPTED

ACCEPTED MANUSCRIPT

a

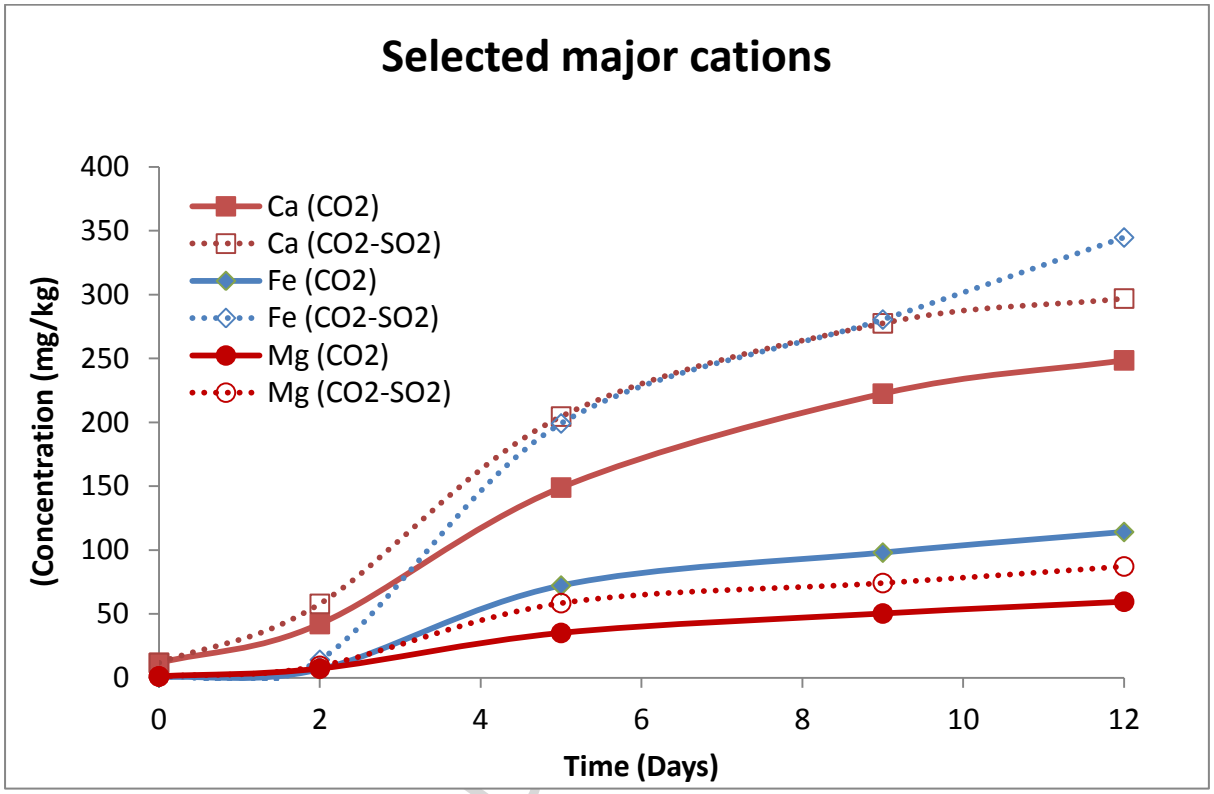

b

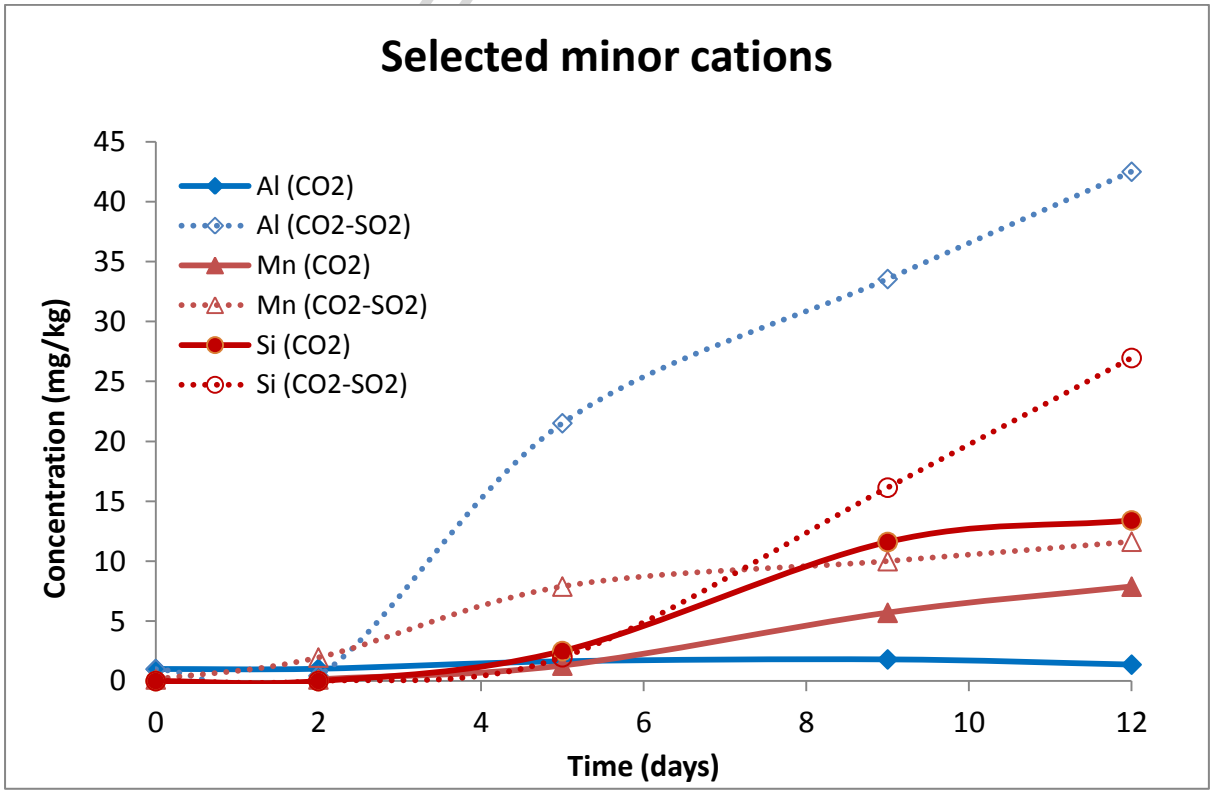

Figure 5

ACCEPTED MANUSCRIPT

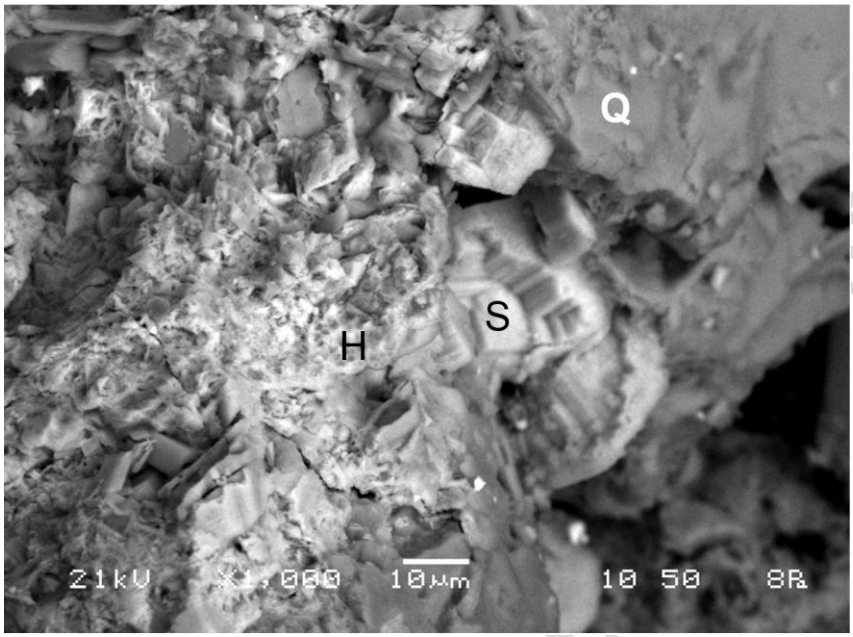

Figure 6a

ACCEPTED MANUSCRIPT

ACCEPTED MANUSCRIPT

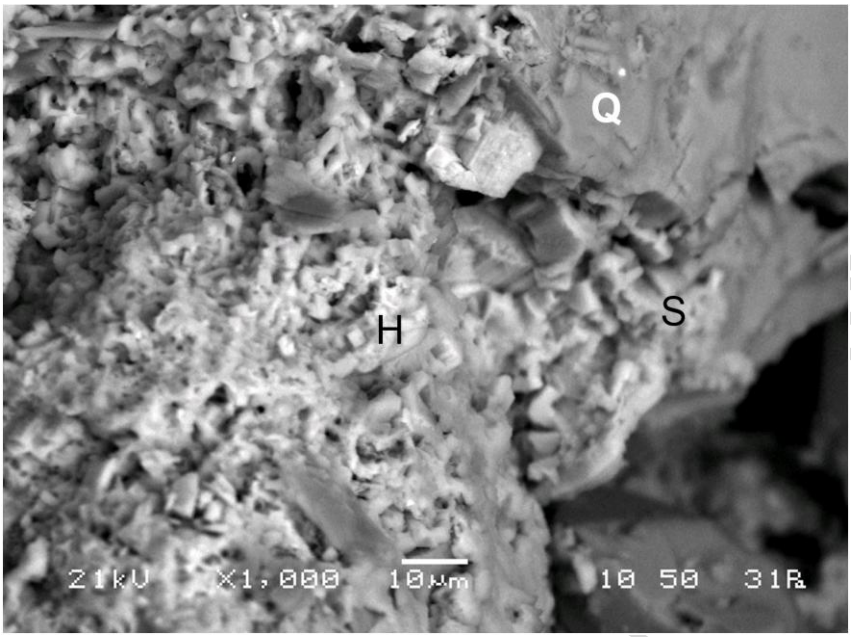

Figure 6b

ACCEPTED MANUSCRIPT

ACCEPTED MANUSCRIPT

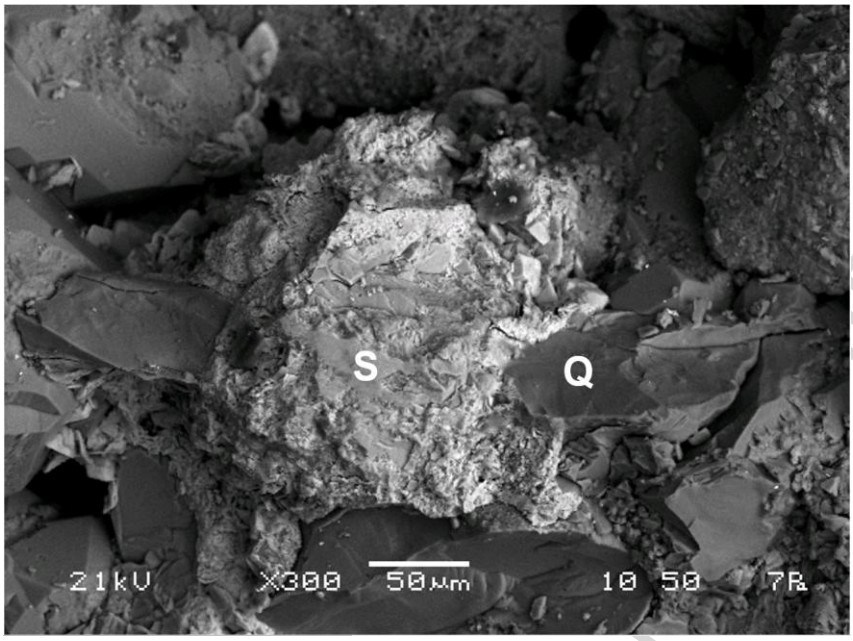

Figure 6c

ACCEPTED MANUSCRIPT

ACCEPTED MANUSCRIPT

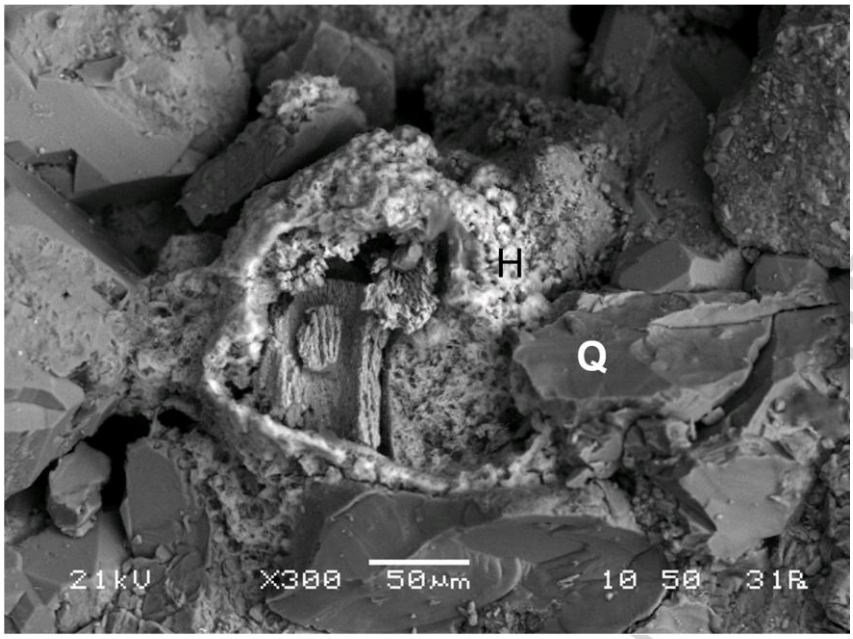

Figure 6d

ACCEPTED MANUSCRIPT

ACCEPTED MANUSCRIPT

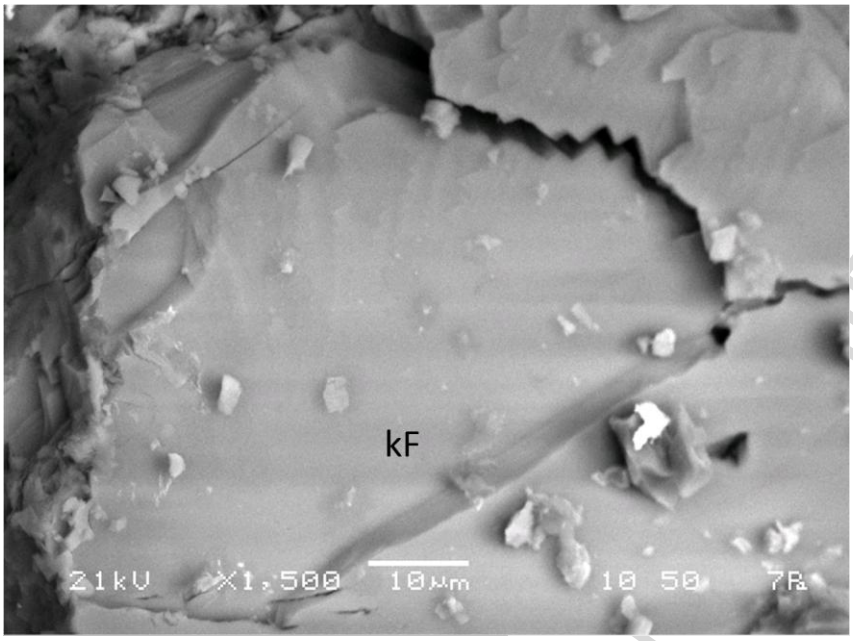

Figure 6e

ACCEPTED MANUSCRIPT

ACCEPTED MANUSCRIPT

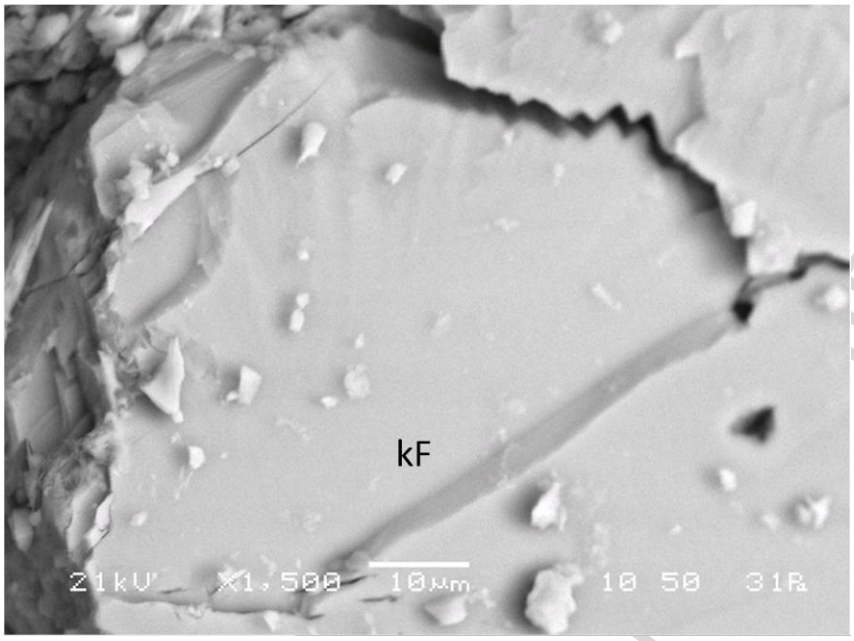

Figure 6f

ACCEPTED MANUSCRIPT

ACCEPTED MANUSCRIPT

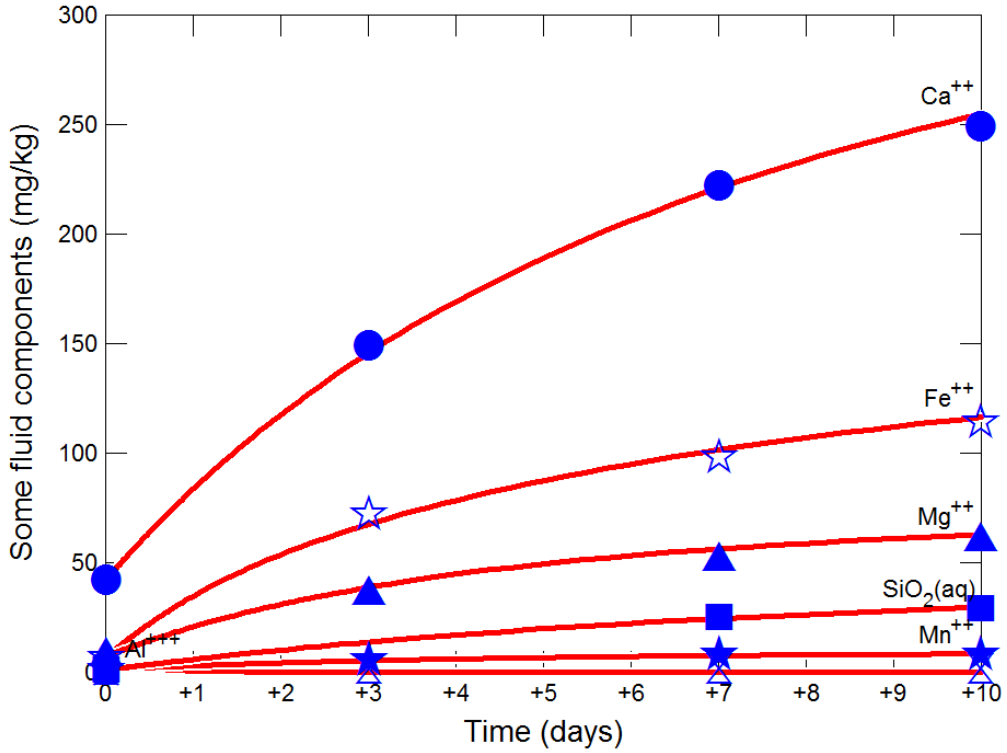

Figure 7a

ACCEPT

ACCEPTED MANUSCRIPT

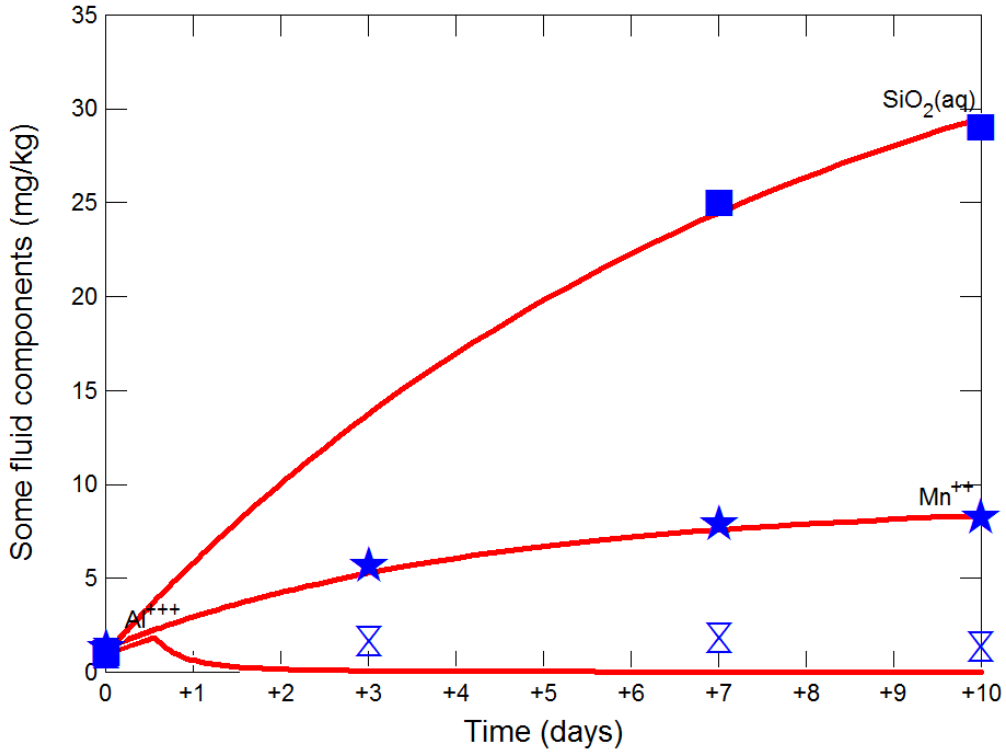

Figure 7b

ACCEPT

ACCEPTED MANUSCRIPT

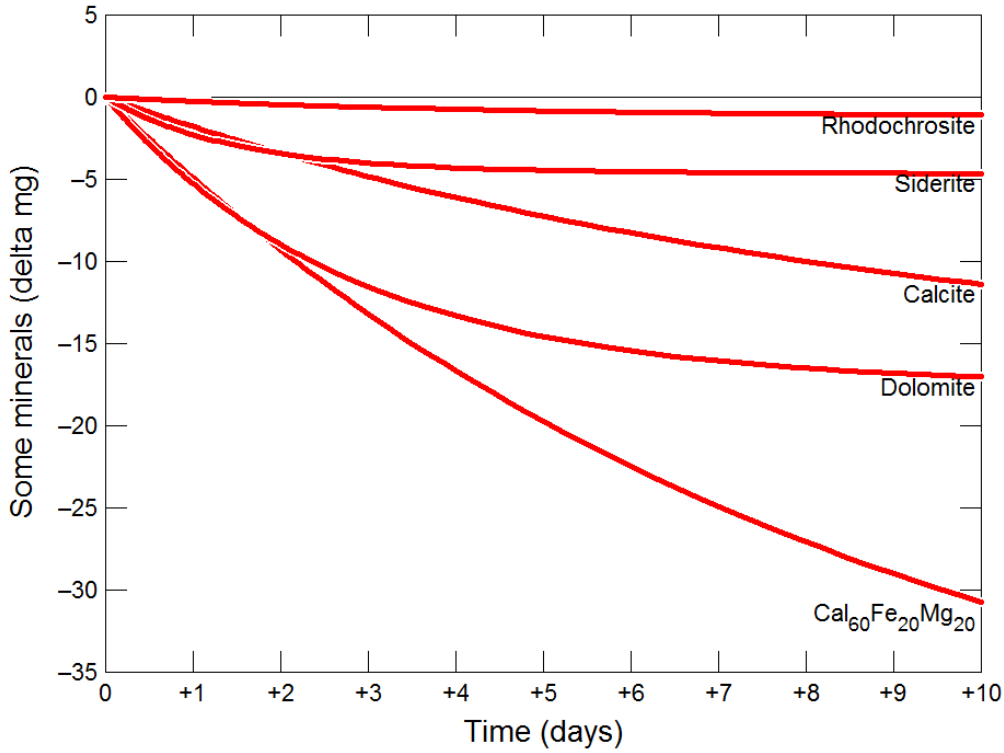

Figure 7c

ACCEPT

ACCEPTED MANUSCRIPT

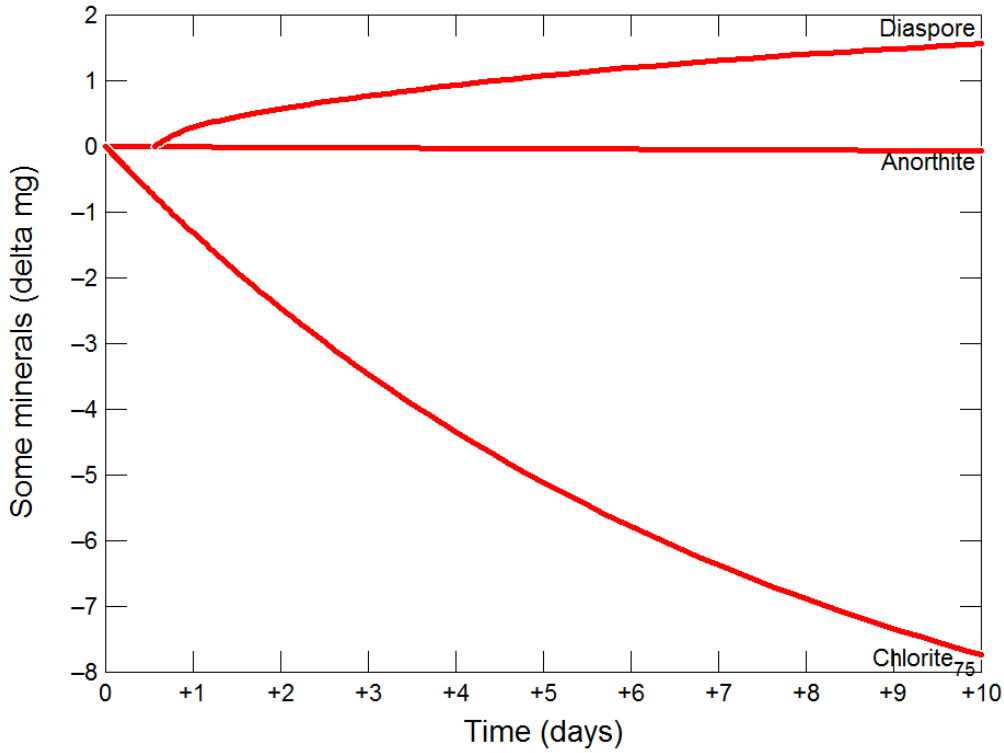

Figure 7d

ACCEPT

ACCEPTED MANUSCRIPT

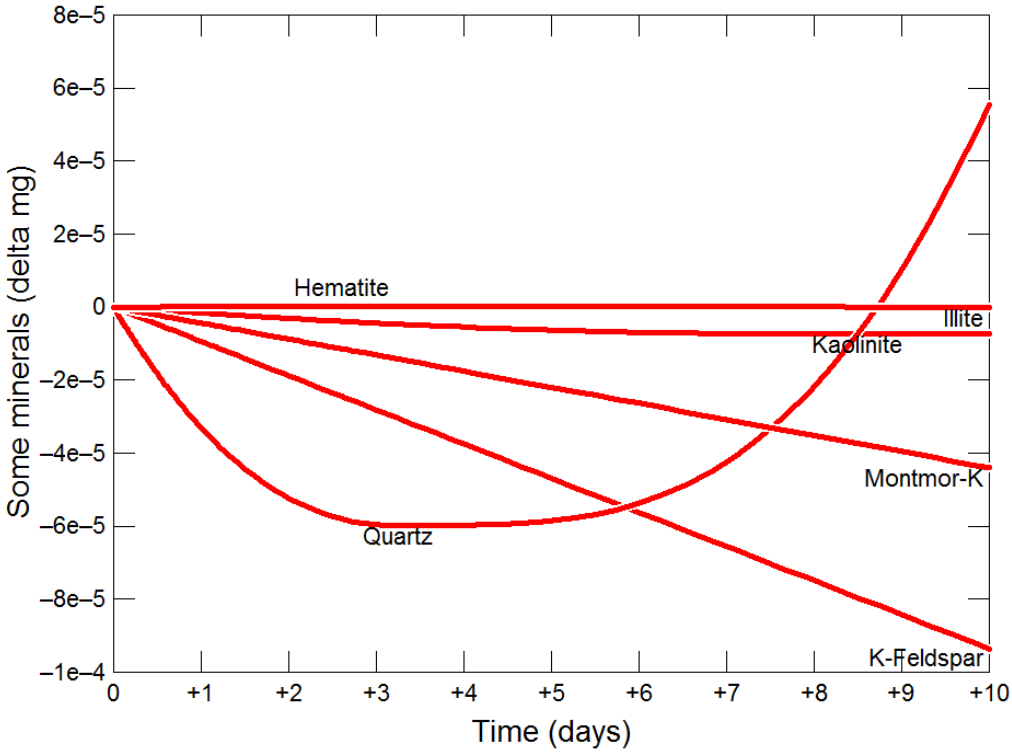

Figure 7e

ACCEPT

ACCEPTED MANUSCRIPT

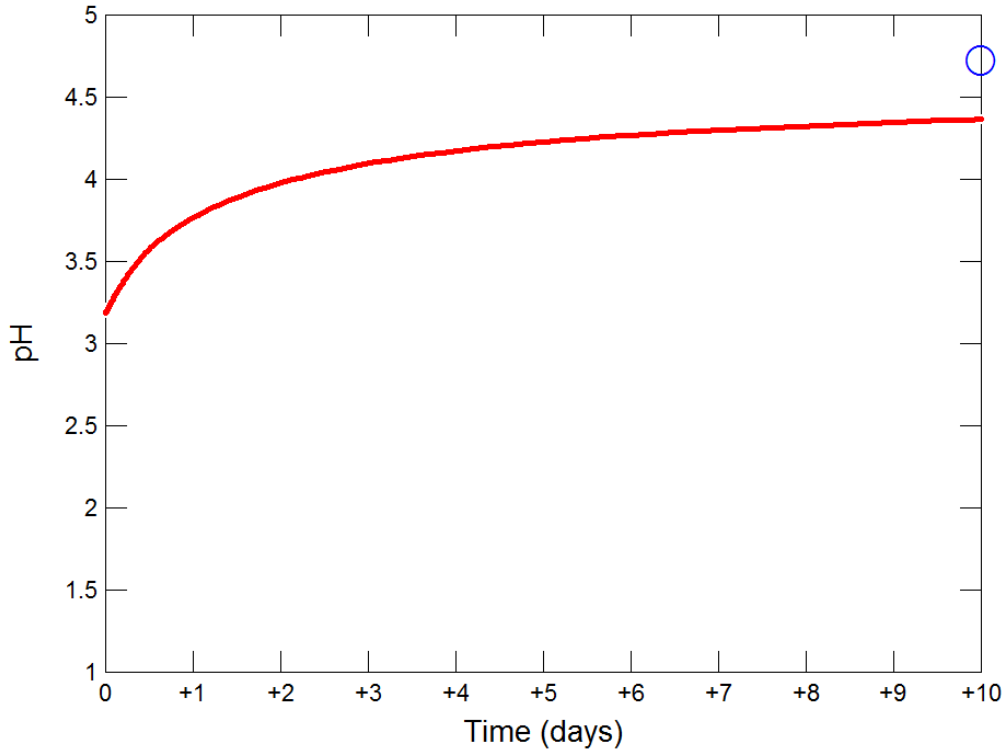

Figure 7f

ACCEPT

ACCEPTED MANUSCRIPT

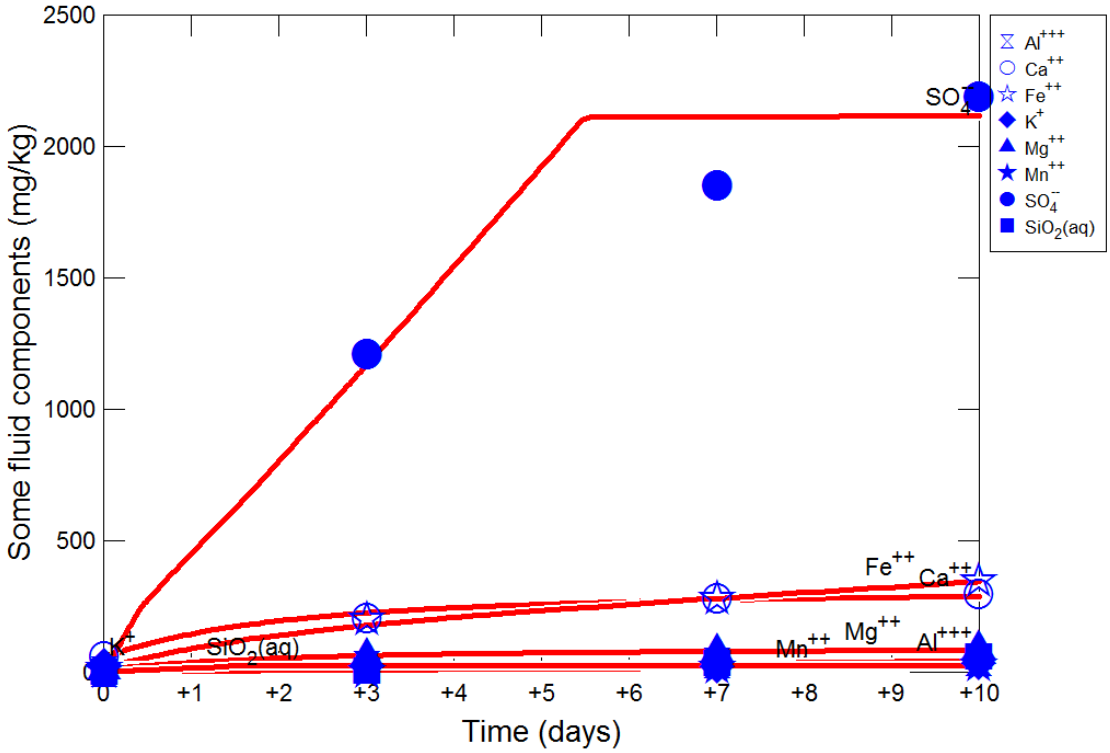

Figure 8a

ACCEPT

ACCEPTED MANUSCRIPT

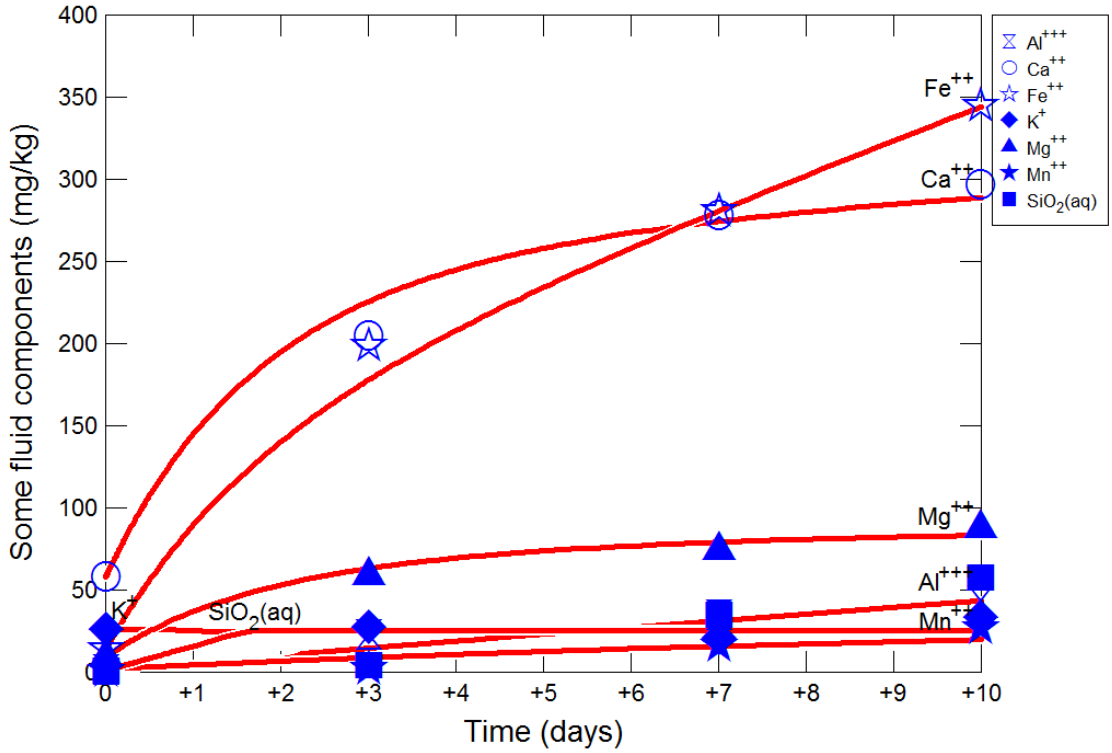

Figure 8b

ACCEPT

ACCEPTED MANUSCRIPT

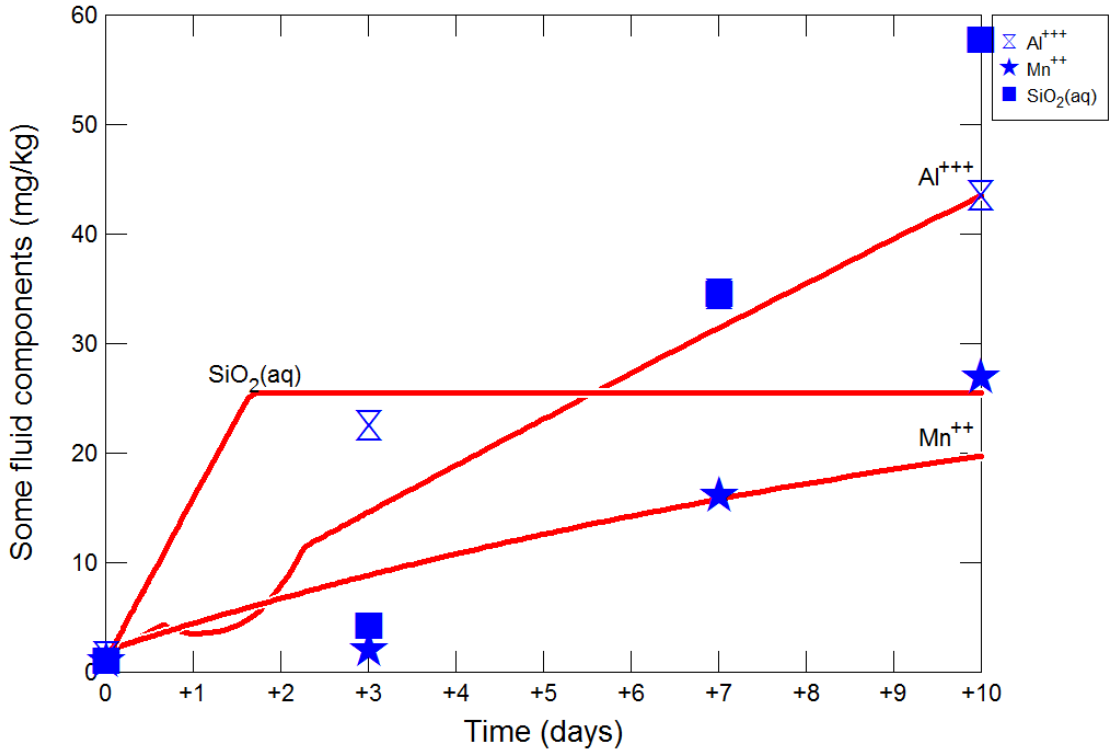

Figure 8c

ACCEPT

ACCEPTED MANUSCRIPT

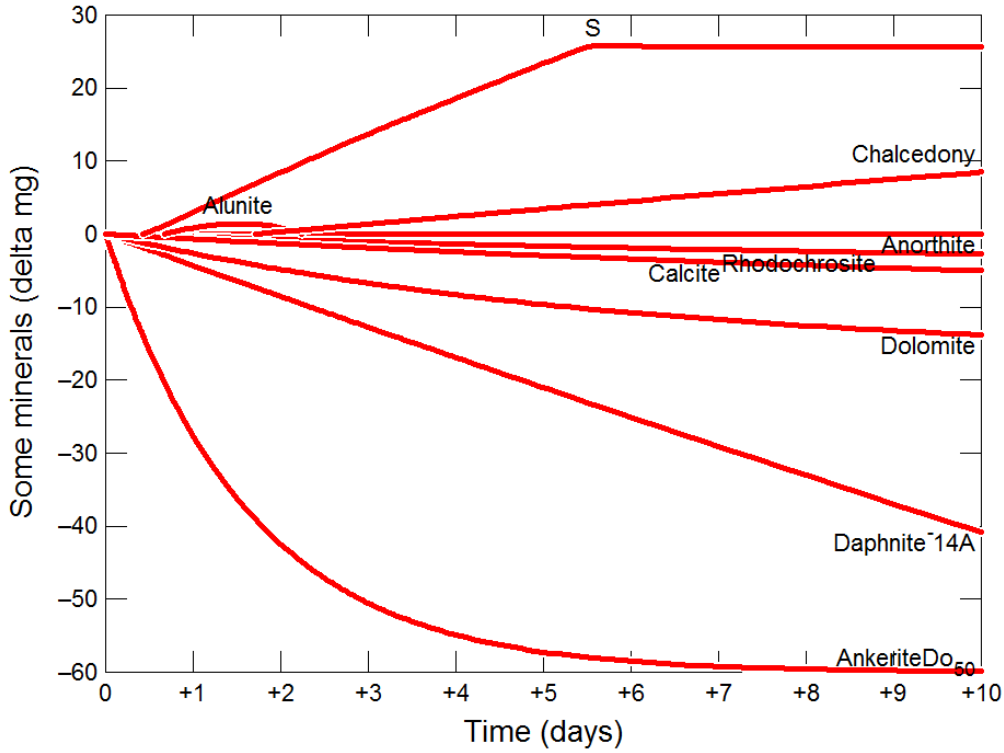

Figure 8d

ACCEPT

ACCEPTED MANUSCRIPT

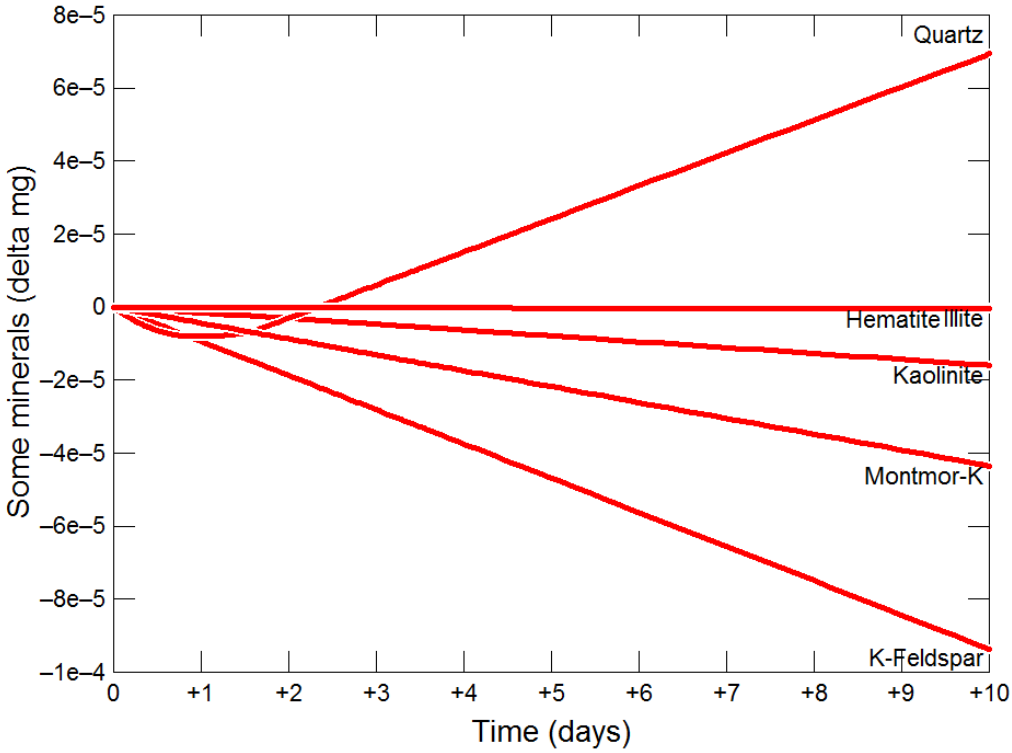

Figure 8e

ACCEPT

ACCEPTED MANUSCRIPT

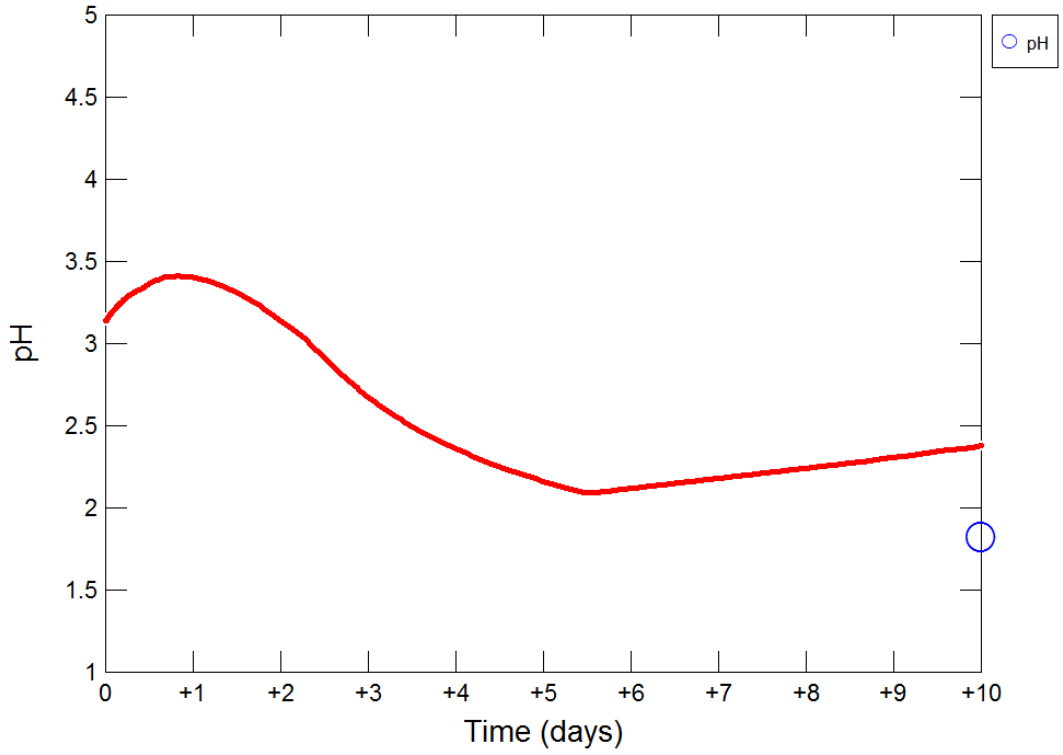

Figure 8f

ACCEPT

ACCEPTED MANUSCRIPT

Table 1: Mineral composition of Berea Sandstone as determined by whole rock and clay separate XRD analysis in this study and others

Minerals	Percentage composition	
	This study	Literature average[a]
Ankerite	0.4	
Anorthite	3.2	n.d.
Calcite	trace	1
Chlorite	trace	0.4
Dolomite	0.2	
Dolomite + Ankerite		2.6
Illite/Muscovite	trace	2
Kaolin	1.6	5.5
K-feldspar	4.1	5
Quartz	90.6	80
Siderite	trace	2.5
Smectite	trace	1

Table 2: The input solution basis used for the models, where cube B was reacted with CO_2-brine, and cube C was reacted with SO_2-CO_2-brine.

Species/Sample	Aqueous and gaseous species model input parameters (mg/kg unless otherwise noted)	
	Cube B	Cube C
H_2O	0.07 (kg) solvent	0.07 (kg) solvent
Al^{3+}	1.01	1.43
Ca^{2+}	42.1	57.9
Cl^-	9095	8468
$CO_{2(g)} \Leftrightarrow H^+$	53.2 (fugacity)	53.2 (fugacity)
Fe^{2+}	6.65	14
HCO_3^-	$5.15*10^{-4}$ (mol/kg) charge balance	$2.579*10^{-4}$ (mol/kg) charge balance
K^+	32.41	26.29
Mg^{2+}	7.17	9.35
Mn^{2+}	1.29	1.96
Na^+	5819	5380.5
$O_{2(g)} \Leftrightarrow O_{2(aq)}$	N/A	-40.0 (log fugacity)
$SiO_{2(aq)}$	1.0055	1.0055
SO_4^{2-}	N/A	0.01

ACCEPTED MANUSCRIPT

Table 3: Kinetic parameters used in geochemical models

Mineral	**$K_{25(acid)}$** mol/cm^2/s	**$E_{a(acid)}$** kJ/mol	**n**	**$K_{25(neut)}$** mol/cm^2/s	**$E_{a(neut)}$** kJ/mol	**$K_{(precip)}$** mol/cm^2/s	**τ**
Amorphous silica	0	0	0	1.70E-17	68.70	$K_{(diss)}$	2E+10
Ankerite	1.59E-08	45.0	0.900	1.26E-13	62.76	$K_{(diss)}$/1e+05	3E+10
Anorthite	3.16E-08	16.6	1.000	7.59E-14	17.80	$K_{(diss)}$	2E+10
Calcite	5.01E-05	14.4	1.000	1.55E-10	23.50	$K_{(diss)}$	1E+10
(Fe-Mg)-Chlorite	1.62E-14	25.1	0.490	1.00E-17	94.30	$K_{(diss)}$	2E+10
Dolomite	6.46E-08	36.1	0.500	2.95E-12	52.20	$K_{(diss)}$	3E+10
Hematite	4.07E-14	66.2	1.000	2.51E-19	66.2	$K_{(diss)}$	3E+10
Illite/Muscovite	1.91E-16	46.0	0.600	8.91E-20	14.00	$K_{(diss)}$	2E+10
Kaolinite	4.90E-16	65.9	0.777	6.61E-18	22.20	$K_{(diss)}$/50	2E+10
K-feldspar	8.71E-15	51.7	0.500	3.89E-17	38.00	$K_{(diss)}$	2E+10
Quartz	0	0	0	3.98E-18	90.90	$K_{(diss)}$	5E+10
Siderite	1.59E-08	45.0	0.900	1.26E-13	62.76	$K_{(diss)}$/50	2E+10
Smectite (K-Montmorillonite)	1.05E-15	23.6	0.340	1.66E-17	35.00	$K_{(diss)}$	2E+10

Table 4: Input mineral mass and surface area in refined models (with initial values in brackets where different to final values)

Reactant/input data	Mass (g)		Surface area (cm^2/g)	
	Cube B	Cube C	Cube B	Cube C
Ankerite ($Ca_{0.6}$-$Mg_{0.2}$-$Fe_{0.2}$)	0.045 (0.027)	N/A	15,000 (10)	N/A
Ankerite (Ca-$Mg_{0.5}$-$Fe_{0.5}$)	N/A	0.06 (0.027)	N/A	40,000 (10)
Anorthite	0.217	0.217	10	10
Calcite	0.017 (0.014)	0.01	40 (10)	25 (10)
Chlorite ($Fe_{3.75}$-$Mg_{1.25}$)	0.0105 (0.027)	N/A	12,100,000 (70)	N/A
Chlorite (Daphnite-14A)	N/A	0.37 (0.027)	N/A	1,000,000 (70)
Dolomite	0.0175 (0.02)	0.017	1500 (10)	700 (10)
Hematite	0.05	0.05	40	40
Illite/muscovite	0.136	0.136	30	30
Kaolinite	0.136	0.136	40	40
K-feldspar	0.306	0.306	10	10
Quartz	5.7911 (5.44)	5.425 (5.44)	10	10
Rhodochrosite[a]	0.0012 (0.007)	0.005 (0.007)	60,000 (10)	20,000 (10)
Siderite	0.0047 (0.17)	N/A (0.17)	75,000 (10)	N/A
Smectite (K-Montmorillonite)	0.068	0.068	40	40

ACCEPTED MANUSCRIPT

Table 5: ICP-OES measured element concentrations (mg/kg) in solution during experiments with CO_2-brine or SO_2-CO_2-brine [a]

Sample / Element[a]	Gas	Day	Al	Ba	Ca	Cd	Cr	Cu	Fe	K	Li	Mg	Mn	Mo	Na	Ni	P	Pb	S	Si	Sr	V	Zn	*ex situ* pH
Stock 1% NaCl solution	N/A	N/A	0.99	<DT	11.7	<DT	0.013	<DT	0.3	22.71	4.24	1.06	0.13	0.09	5194	<DT	3.27	<DT	<DT	<DT	1.12	0.64	<DT	
Pure water blank	CO_2	4	0.16	<DT	1.79	<DT	0.090	0.14	0.57	0.21	0.052	0.16	0.17	<DT	8.59	0.103	0.08	0.0049	<DT	0.47	0.059	0.0093	0.18	
Blank experiments with 1% NaCl	N_2	11	2.82	0.441	14.4	0.14	0.647	0.20	3.97	27.53	4.22	1.87	0.68	0.21	6184	1.31	2.81	<DL	<DL	<DL	1.12	0.73	0.78	
	CO_2	11	0.95	<DT	13.20	<DT	0.539	0.0050	3.42	23.85	4.10	0.25	0.18	0.19	5514	0.26	3.27	<DT	<DT	0.47	1.06	0.74	0.085	
	SO_2-CO_2	11	1.04	<DT	12.9	0.20	5.09	0.22	14.82	29.16	3.84	0.071	0.51	0.17	5424	2.76	3.16	<DT	439	0.25	1.32	1.16	1.57	
Berea A	CO_2	15	<DT	0.079	145.3	0.088	0.11	<DT	80.59	6.33	<DT	41.23	5.44	<DT	5933	0.87	<DT	<DT	<DT	3.88	0.078	<DT	0.52	5.77
Berea B	N_2	2	1.01	<DT	42.1	<DT	0.13	0.30	6.65	32.41	4.16	7.17	1.29	0.11	5819	0.01	3.23	<DT	<DT	<DT	1.07	0.68	<DT	
	CO_2	5	1.64	<DT	149	<DT	0.68	0.70	72.2	22.13	4.26	35.13	5.69	0.17	5799	1.92	3.54	<DT	<DT	2.50	1.22	0.81	0.32	
		9	1.80	<DT	222	<DT	0.21	0.60	98.0	25.04	4.03	50.35	7.88	0.20	5953	1.33	2.88	<DT	<DT	11.60	1.17	0.94	0.29	
		12	1.37	<DT	249	<DT	0.15	0.43	114	27.28	3.84	59.60	8.26	0.15	5889	0.48	3.28	0.06	<DT	13.40	1.20	0.84	0.50	4.72
Berea C	N_2	2	1.43	<DT	57.9	<DT	0.26	0.33	14.0	26.29	4.11	9.35	1.96	0.18	5395	0.28	3.02	<DT	<DT	<DT	1.11	0.70	2.07	
	SO_2-CO_2	5	22.5	<DT	205	<DT	3.34	0.63	199	27.76	4.23	58.48	7.89	0.47	6003	1.95	3.47	0.08	403	1.99	1.19	0.94	1.44	
		9	34.5	<DT	278	<DT	5.55	0.53	281	20.46	4.06	74.18	10.01	0.34	5752	3.23	2.55	0.20	618	16.14	1.24	1.03	1.46	
		12	43.5	<DT	297	<DT	8.21	0.16	345	33.50	3.96	87.17	11.63	0.38	5706	6.68	2.62	0.15	730	26.96	1.23	1.14	1.75	2.69

ACCEPTED MANUSCRIPT

ACCEPTED MANUSCRIPT

Table 6: Mineral mass changes for Cube B CO_2-brine model after 10 days reaction

	Weight			Amount reacted[a]	
	Initial		Final		
Reactants	(%)	(g)	(g)	(g)	(%)
Ankerite	0.66	0.045	0.0143	3.07E-02	68.29
Anorthite	3.19	0.217	0.2169	6.89E-05	0.032
Calcite	0.25	0.017	0.0056	0.01137	66.88
(Fe-Mg)-Chlorite	0.15	0.0105	0.0028	0.007733	73.65
Dolomite	0.26	0.0175	0.0005	0.01701	97.2
K-feldspar	4.5	0.306	0.3060	9.36E-08	3.06E-05
Hematite	0.75	0.05	0.0500	3.94E-11	7.89E-08
Illite/muscovite	2	0.136	0.1360	1.87E-10	1.37E-07
Kaolinite	2	0.136	0.1360	7.44E-09	5.47E-06
Quartz	85.2	5.7911	5.7911	-5.55E-08	-9.58E-07
Rhodochrosite	0.02	0.0012	0.0001	0.001084	90.33
Siderite	0.07	0.0047	0.0001	0.004644	98.81
Smectite (K-Montmorillonite)	1	0.068	0.0680	4.40E-08	6.47E-05

Table 7: Mineral mass changes for Cube B SO_2-CO_2-brine model after 10 days reaction

	Weight (g)			Amount reacted[a]	
	Initial		Final		
Reactants	(%)	(g)	(g)	(g)	(%)
Ankerite	0.88	0.06	0.0001	5.99E-02	99.78
Anorthite	3.19	0.2167	0.2166	6.89E-05	0.032
Calcite	0.15	0.01	0.0050	0.00502	50.2
Chlorite (Daphnite-14A)	5.44	0.37	0.3292	0.04083	11.04
Dolomite	0.25	0.017	0.0032	1.38E-02	81.24
K-feldspar	4.5	0.306	0.3060	9.37E-08	3.06E-05
Hematite	0.74	0.05	0.0500	5.47E-10	1.09E-06
Illite/muscovite	2	0.136	0.1360	1.87E-10	1.37E-07
Kaolinite	2	0.136	0.1360	1.59E-08	1.17E-05
Quartz	79.8	5.425	5.4250	-6.94E-08	-1.28E-06
Rhodochrosite	0.07	0.005	0.0023	0.002739	54.78
Smectite (K-Montmorillonite)	1.00	0.068	0.0680	4.35E-08	6.40E-05
SO_2(g)				0.1552	100

ACCEPTED MANUSCRIPT

Highlights

- Greater mineral dissolution during SO_2-CO_2-brine experiments compared with CO_2-brine
- Mineral behaviour shown via SEM images of identical spots pre and post experiment
- Geochemical modelling indicated that chlorite reacted during all experiments

ACCEPTED MANUSCRIPT